POLITECNICO DI TORINO
Repository ISTITUZIONALE

Sensitivity driven model updating: a multi-step procedure for structural assessment

Original
Sensitivity driven model updating: a multi-step procedure for structural assessment / Lenticchia, E., Miraglia, G., Cusicanqui Lopez, J.A., Ceravolo, R.. - In: JOURNAL OF BUILDING ENGINEERING. - ISSN 2352-7102. - 109:(2025), pp. 1-23. [10.1016/j.jobe.2025.112941]

Availability:
This version is available at: 11583/3000730 since: 2025-06-06T12:52:32Z

Publisher:
Elsevier

Published
DOI:10.1016/j.jobe.2025.112941

Terms of use:

This article is made available under terms and conditions as specified in the corresponding bibliographic description in the repository

Publisher copyright

(Article begins on next page)

19 November 2026

Journal of Building Engineering 109 (2025) 112941



Contents lists available at ScienceDirect

Journal of Building Engineering

journal homepage: www.elsevier.com/locate/jobe



Sensitivity driven model updating: a multi-step procedure for structural assessment

Erica Lenticchia [a,b,*], Gaetano Miraglia [a,b], Jorge Alexis Cusicanqui Lopez [a], Rosario Ceravolo [a,b]

[a] Department of Structural, Building and Geotechnical Engineering, Politecnico di Torino, Corso Duca Degli Abruzzi 24, 10129, Turin, Italy
[b] Responsible Risk Resilience Interdepartmental Centre (R3C), Politecnico di Torino, Corso Duca Degli Abruzzi 24, 10129, Turin, Italy

ARTICLE INFO

Keywords:
Digital twin
Historical buildings
Inspection and diagnosis
Model calibration
Sensitivity analysis

ABSTRACT

Automatic model updating, or model calibration procedures, have significantly streamlined the creation of digital twins, i.e., virtual models strongly informed by experimental data. This methodology supports real-time monitoring and predictive maintenance by ensuring the digital twin accurately reflects the physical structure. However, when the parameters to be inferred are modal parameters, such as natural frequency or mode shape, additional challenges arise. This is especially true in the case of complex monumental buildings. A key issue is ensuring the model not only predicts these parameters correctly but also in the same order as seen in Operational Modal Analysis campaigns. Discrepancies in predicted versus experimental modal parameters often indicate significant modeling errors, resulting in inversions of the predicted vibrational modes. These inversions can invalidate automatic model updating results, slowing the calibration process and leading to potentially incorrect results. Several factors can cause these mode inversions, including inaccuracies in model parameters or modeling simplifications. This work introduces a procedure to mitigate the mode inversion problem by leveraging sensitivity analysis to select the most impactful mechanical parameters and vibration modes for calibration. The proposed methodology involves initial mechanical testing to reduce parameter uncertainties, followed by sensitivity analysis to identify key parameters. Preliminary model assessment and mode matching are then conducted to establish baseline discrepancies. Sensitive parameters are adjusted to align the model more closely with experimental data, followed by a recursive calibration process. The updated model is validated and verified against Operational Modal Analysis results, ensuring correct ordering and reduced errors of modal parameters.

1. Introduction

Assessing the health state of a monumental building that belong to the architectural heritage is not a trivial matter. Even without considering the effect of possible degradation phenomena on the health state of these buildings, the level of uncertainties related to the actual knowledge of the mechanical properties of the materials, the levels of connections of the structural elements are very high [1].

A critical aspect of understanding the structural behavior of physical systems is identifying the causes and measuring the effects of varying mechanical parameters [2]. However, conducting this task on an actual structure would require drastic alterations to its

* Corresponding author. Corso Duca degli Abruzzi 24, 10129, Torino, Italy.
E-mail address: erica.lenticchia@polito.it (E. Lenticchia).

https://doi.org/10.1016/j.jobe.2025.112941
Received 23 September 2024; Received in revised form 16 May 2025; Accepted 18 May 2025
Available online 22 May 2025
2352-7102/© 2025 The Authors. Published by Elsevier Ltd. This is an open access article under the CC BY license (http://creativecommons.org/licenses/by/4.0/).

structural characteristics. To overcome this challenge, a virtual model can be designed for the purpose of studying and analyzing these parameters [3–5]. Models may help in reducing these uncertainties by supplementing some mechanical behavior hypothesis; however, it is crucial to choose the proper parameters to create a reliable model. Uncertainties may be reduced by providing information coming from experimental campaigns carried out on the structure under analysis. This approach allows for a more efficient and effective way to gain insights into the complex behavior of physical systems without the need for costly and time-consuming physical alterations. However, when dealing with heritage building is not always possible to carry out all the necessary investigations: this is due to the lack of funds, the large complexity of the building under analysis, or the fact that destructive tests cannot be always employed, since they may destroy some vital component that needs to be preserved [6,7]. Additional information may be provided by non-destructive testing [8,9], although, for the estimation of the mechanical parameters, they are usually affected by higher levels of uncertainties.

When dealing with a large number of parameters to be optimized [10], the validation process of the numerical model can be quite daunting [11–13]. The extensive computational burden required to achieve this objective is often unsustainable. However, conducting a Sensitivity Analysis (SA) targeted at determining the influence of model parameters on experimental data predictions can immensely reduce this computational burden. This, in turn, allows for a redirection of efforts to where they are most needed, consequently increasing efficiency and effectiveness. Sensitivity is thus a key tool in civil engineering, and it was used in the past to solve different problems. For instance, SA, as mentioned, is crucial in calibrating civil-engineering numerical models (e.g., finite-element models), identifying which parameters most affect structural response [14]. It guides calibration by highlighting key variables to adjust, improving agreement with experimental data. SA methods are broadly classified as deterministic (local derivative-based) or stochastic (global, variance-based) approaches [15]. In practice, SA informs parameter selection: for example [16], use sensitivity measures to choose important stiffness or mass parameters in a space-frame model. Early SA-based updating used Frequency-Response Functions (FRF) [17], though such FRF methods had limitations. Later approaches combine SA with modal constraints: e.g., [18] employ eigenvalue sensitivities for constrained FE updating. These ideas span linear and nonlinear contexts. Sobol variance analysis was used for nonlinear steel-frame design [19,20] demonstrate a manual SA-guided updating of a cable-stayed bridge. More recently [21], apply sensitivity-based FE updating in nonlinear seismic analyses of heritage structures. In all cases, SA-driven updating refines models to better match observations [14,20,21].

The present paper proposes a framework for model verification and validation based on sensitivity analysis; in particular, it focuses on a proposal for assessing the structural health state through diagnosis data coming from an extensive experimental campaign and the creation of the optimal digital twin. In order to do so, the paper presents the various steps on a monumental building built in the first half of the 20th century.

The paper is structured as follows: In Section 2 the proposed methodology approach is described. Section 3 reports the experimental campaign carried out, while in Section 4 the digital twin of the reference structure is described. In Section 5, the main results of the study are discussed. Finally, in Section 6 the conclusions of the work are drawn.

1.1. Research significance

When working on very complex structures, the validation process of the virtual model is of fundamental importance, as it will give rise to the results of more in-depth analyzes aimed at evaluating the level of degradation, damage [22], or more generally the health state of the structure. However, the process of verifying and validating a numerical model of very complex structures can be onerous, and very often the computational burden necessary to achieve this goal is unsustainable. Through a sensitivity analysis aimed at defining the impact that the model parameters have on the predictions of experimental data, it is possible to drastically reduce this computational burden, which allows the effort to be moved to where it is really needed.

In the present article, the verification and validation of the numerical model is addressed through the use of modal model updating methods, using different objective functions for different sets of mechanical parameters. In this way, it is possible to associate more significant objectives with mechanical parameters that modify specific dynamic aspects. For example, the mechanical parameters that mostly regulate the flexural behavior of the structure are inferred using inverse techniques that include in the objective function only modal parameters (e.g., modes of vibration) that have flexural characteristics. This involves a decoupling, where possible, of the inverse problem and therefore greater robustness and accuracy of the results, combined with an increase in computational efficiency. To do so, after performing the sensitivity analysis, a mode matching selection is needed, with the aim to place in the correct order the numerical and experimental vibration mode and avoid error propagation during the updating due to the mismatching of the pairing.

2. Methodology

The automatic model updating, or model calibration procedures, have made it possible to facilitate the twinning phase of a virtual model, i.e., the process through which a digital model is informed starting from data collected on a structure equipped with sensors [23]. This digital twin approach allows for real-time monitoring [3,24–26] and predictive maintenance by ensuring that the virtual model closely mirrors the physical structure. However, when the parameters to be inferred through the use of the model are modal parameters (e.g., natural frequency or mode shape), there are additional challenges. Beyond the common issues associated with other types of data, there is the critical problem of ensuring that the comparison between the model and reality is coherent. This means not only verifying that the model correctly predicts the modal parameters but also ensuring that it provides these results in the same order as observed from the Operational Modal Analysis (OMA) campaigns [27–29]. When the predicted modal parameters do not align with the experimental data, it can indicate excessive modeling discrepancies. These discrepancies arise from initial conditions in the model (such as the configuration of mechanical and geometric parameters) that are too far from the real conditions of the structure. This

misalignment often results in an inversion of the predicted vibrational modes. Consequently, the automatic model updating techniques become unreliable, leading to slow calibration processes that require numerous cycles to reach convergence and yield results that may still be incorrect due to the inability to correctly pair numerical predictions with experimental evidence.

In more detail, when the vibration modes are reversed, the modes expected to see at one natural frequency appear at a different frequency, and vice versa. This can occur for several reasons.

- Inaccuracies in model parameters: if model parameters, such as stiffness or mass, are not accurately defined, predicted vibration modes may not correspond to the correct frequencies.
- Modeling effects: simplifying assumptions or incomplete models can lead to incorrect predictions of modal frequencies.
- Discretization errors: in finite element modeling, the discretization of the structure can affect the accuracy of the predicted modes.
- Boundary conditions: errors in the definition of boundary conditions can cause significant discrepancies in the vibration modes.

To address the mode reversal problem, several tools can be used. The Modal Assurance Criterion (MAC) can be used to verify the correlation between numerical and experimental mode shapes. If the modes are reversed, the MAC may detect a low correlation between the predicted and observed mode shapes, signaling the need for further investigation. The analysis of mode curvatures can provide additional information on the correctness of the pairing. More specifically, curvature analysis can help identify reversals by observing anomalous changes in the shape of the vibration modes. Iterative model updating process can help identify and correct reversals vibration modes. In this case the model parameters are updated step by step and at each iteration, the updated mode shapes are compared with the experimental ones to verify improvements.

The present work proposes a procedure to alleviate the problem of mode inversion. This approach leverages the concept of sensitivity analysis [30] in selecting mechanical parameters and vibration modes for use in calibration processes. Sensitivity analysis helps identify which parameters have the most significant impact on the model's accuracy, allowing for more targeted and effective updates. The methodology aims to reduce discrepancies between the virtual model and the real structure, resulting in a more reliable numerical reference model for future advanced calibration activities. The procedure is structured as follows.

1. **Mechanical testing**: Perform preliminary mechanical test in order to reduce uncertainties in model parameters values (increase the knowledge of the structure).
2. **Sensitivity analysis**: Perform a sensitivity analysis to determine which mechanical parameters and vibration modes have the most significant influence on the model accuracy.
3. **Preliminary assessment and Mode matching**: Conduct a preliminary analysis of the virtual model informed with mechanical tests results to identify the baseline discrepancies between the predicted and experimental modal parameters.
4. **Targeted *variable inputs* adjustment**: Adjust the identified sensitive parameters to better align the model with the experimental data, reducing the risk of mode inversion.
5. **Recursive updating of *calibration inputs***: Implement a recursive calibration process using the updated parameters to refine the model progressively.
6. **Validation and verification**: Validate the updated model by comparing its predictions with OMA outcomes and verify that the order of the predicted modal parameters matches the experimental observations, with reduced errors of modal parameters values if compared with the initial configuration.
7. **Final model deployment**: Once validated, use the updated model as a reference for ongoing monitoring and future automatic calibration activities.



(a) (b)

Fig. 1. Views of the Hall B structure (picture (a) is courtesy of Fabio Oggero) (Rosario [33]).

3. Structural testing and diagnosis

An extensive review of historical documentation is a fundamental step for helping in the identification of unique features and material variations across all structural elements. This enables the formulation of a minimally invasive testing strategy, by combining targeted sample extraction with non-destructive testing techniques. In the following subsections a description of the case study and the experimental campaign is presented. This information constitutes our benchmark model and the dataset for the model verification and validation based on sensitivity analysis.

3.1. The benchmark building

The case study used to apply the methodologies presented in this paper is the hall B of Torino Esposizioni, built by Pier Luigi Nervi in 1947-53. The hall is a complex monumental building in concrete and a spatial structure masterpiece, admired for its daring and innovative conception introduced by the designer. Recently Nervi's structures in Torino Esposizioni, which have been abandoned for a long period, apart sporadic and temporary use, have been the object of an extensive investigation and diagnosis campaign to outline the best conservation strategies and its reuse [31,32]. The building, in fact, will host the new civic library of the city. Fig. 1 depicts a view of the benchmark building.

The understanding of the constructive and transformative phases of historical or existing buildings is a crucial step in the definition of the path of knowledge, followed by the identification of each part characterizing the entire complex, an essential starting point for defining an effective testing campaign. For a comprehensive analysis of Hall B's construction history and configuration, refer to [34, 35], while the geometrical documentation and the very-high-scale photogrammetric documentation to generate a multi-scale 3D model are reported in [36,37].

As it can be noticed in Fig. 1, the hall is symmetrical on one axis, and presents a modular system constituted by the repetition of structural elements. This modularity allowed to reduce the duration of the construction site, but also allowed rapid expansion in a short period of time: in fact, in its first configuration (the construction site started in August 1947 and the first part of the structure was completed in May1948), the building measured 96 m in width and 110 m in length. Between 1952 and 1954, Hall B was enlarged by five spans to move the façade on the main street, and it reached the length of 155 m (see Fig. 2). Considering the time needed to complete the first part, it is important to highlight that a large portion of the construction site was carried out during winter, which the standards of the time, the Royal Decree No. 2229 [38], did not recommend as an ideal weather condition for pouring concrete: e.g. the same standards prohibited the installation of conglomerates at rigid temperatures (0 °C for "standard" conglomerates). Moreover, different casting stages interested the monolithic elements such as the inclined pillars, that were cast vertically in different months (see Fig. 2).

3.2. Experimental campaign

The extensive review of the historical documentation allowed the identification of the distinctive features and material differences of all structural elements in order to formulate the least invasive testing campaign possible, combining sample extraction with non-destructive testing.

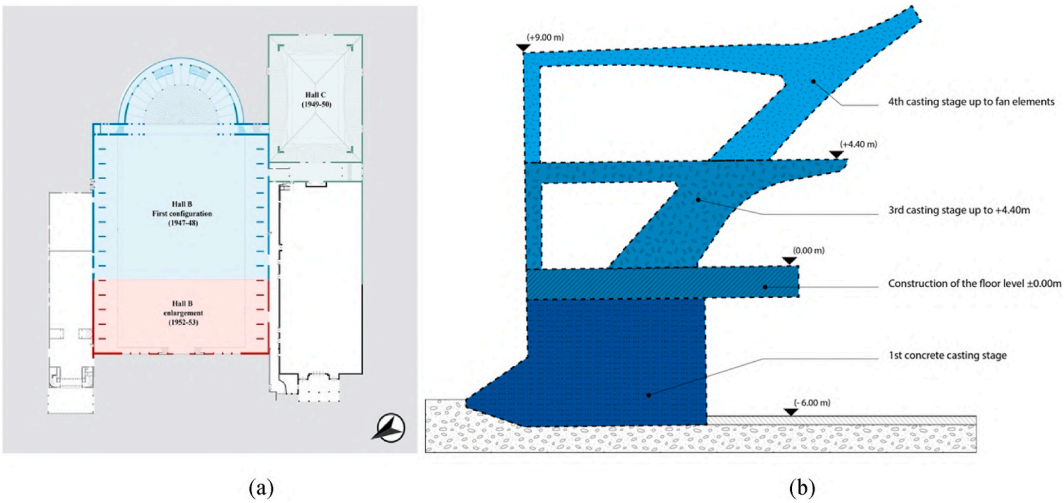


Fig. 2. Schematization of the main construction phases of the Turin exhibition complex (a). Scheme of the various casting stages of the main slanted pillars (b) [32].

3.2.1. Mechanical testing

The sampling for the mechanical tests was limited to the most massive elements, such as the slanted pillars and the beams, and the thin pillars of the apse (see Fig. 1). Identifying potential variations in conglomerate types due to different pouring stages and construction site requirements was a key objective in sample selection. Consequently, core sampling was strategically targeted at locations exhibiting visible dissimilarities. In fact, considering the construction sequence of the hall, which started from the apse in 1947 and continued toward the front on Corso Massimo d'Azeglio (see Fig. 2), it was decided to distribute the tests to investigate the construction progression and detect any substantial differences. The tests were repeated on the different levels (basement, ground floor, balcony floor and finally the roofs) to investigate any anomalies due to different casting phases performed at different times and/or with different conglomerates, if any, taking into consideration the fact that at that time, concrete was manufactured and amalgamated on-site.

Concrete sampling was carried out and prepared according to the EN 12504–1:2019 [39] and EN 12504-1[39] standards by adopting the coring method using diamond crown probes in the constant presence of water. Both compressive strength tests and elastic modulus of elasticity were conducted, by applying an axial load with constant speed, until failure was reached. The value of the elastic modulus was determined according to the requirements of EN 12390–13:2021 [40] method B. The results of the tests are shown in Table 1.

By analyzing the results obtained from the extracted samples, a preliminary analysis can be carried out to check for the presence of different types of concretes, whether these differences are due to different casting stages, different static roles of structural elements, or the difference in material due to the expansion of 1953. Fig. 3 (a), shows the results of the acquired samples in terms of Young Modulus as a function of the compressive strength. It can be observed that the distribution of the results follows the values of the EN1992-1-1:2023 Eurocode 2 [41]. However, given the large distribution in terms of compressive strength, from 20 MPa to 50 MPa, some clusters with the same characteristics could emerge. Considering that, at the time, concrete with different mechanical properties could be employed without necessarily disclosing their presence or precise location in the design drawings (also since some documents could be missing), the presence of different concrete was considered a possibility. In order to investigate possible groups of concrete with similar characteristics, several aspects where investigated, such as the stage of construction, the structural elements, etc. From this first differentiation, Fig. 3 (b), it is possible to state that the properties of 1947 look evenly distributed; however, two different groups can be identified in the expansion of 1953, one with higher values of compressive strength (around 45 MPa), and a second one with lower resistance (between 21 and 26 MPa). Fig. 3 (c), shows that differences are not related to the portion of the building oriented in the northern or southern part, while in Fig. 3 (d), emerges a possible cluster related to the column of the apse. In the same figure, it can be stated that the concrete of the beam elements seems to have a lower variance than the one employed for the slanted pillars. Fig. 3 (e), highlights that differences are not related to the different stages of the construction site. On the other hand in Fig. 3 (f), it emerges that the samples of the higher floor (between the height of 4.40 and 9.00 m), seem to have higher values compared to the ones coming from lower floors. *For comparison of the colors in the figures, the reader can refer to the electronic version of the paper.*

Further investigation permitted the identification of mechanical differences by distinguishing first from the older part of 1947 and the expansion (Fig. 4) and then by identifying the clusters of the columns of the apse and the two additional clusters representing the different floors in the expansion of 1953. In the end, four different clusters (Fig. 5) were determined.

3.2.2. Vibration-based testing

Dynamic testing offers different advantages for heritage structures; they allow capturing the whole-body response of the entire structure, leveraging insights from local inspections, and provide valuable information about seismic behavior and indirectly assessing

Table 1
Core testing results, the ones with the asterisk (*) are related to samples extracted from the extension built in 1953.

Test code	Floor	New/old	Young's modulus [MPa]	Density [kg/m^3]	Compressive strength [MPa]
PI_P13n_C18	−1	old	33804.35	2346	31.7
PI_CI-21_C19	−1	old	26918.88	2255	23.4
PT_P13s_C12	0	old	27083.54	2308	20.6
PT_P8s_C13	0	old	41591.9	2410	49.0
PT_P2s_C14*	0	new	28506.69	2449	21.0
PT_P11n_C15	0	old	30922.15	2372	23.4
PT_P8n_C16	0	old	34922.2	2352	43.9
PT_P2n_C17*	0	new	26750.79	2340	25.8
PT_CI-17_C20	0	old	28853.7	2268	21.8
P1_P13s_C1	1	old	31669.55	2308	32.7
P1_T13s_C2	1	old	31156.1	2341	26.7
P1_P8s_C3	1	old	32566.83	2346	24.4
P1_T8s_C4	1	old	33797.72	2512	37.4
P1_P2s_C5*	1	new	31233.75	2341	44.2
P1_T2s_C6*	1	new	36784.01	2374	41.3
P1_P11n_C7	1	old	35536.94	2385	32.4
P1_T11n_C8	1	old	33921.83	2396	39.0
P1_P8n_C9	1	old	26473.21	2279	21.1
P1_T8n_C10	1	old	31787.57	2350	30.4
P1_P2n_C11*	1	new	32954.22	2374	45.9

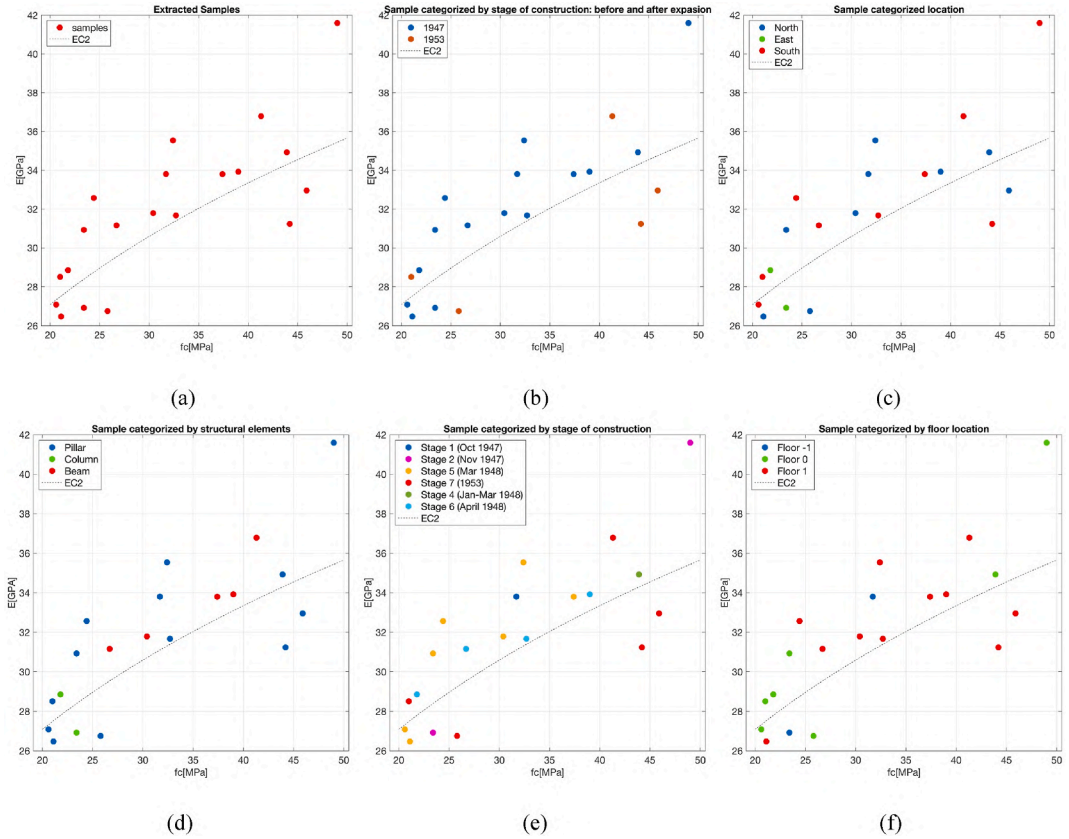


Fig. 3. Analysis of the experimental data by considering the various factors of variations, such as the stage of construction, the vertical location, the structural elements, the construction site stages, and the location in the northern or southern portion of the building. The EC2 represents the Eurocode relationship of the Young's modulus as a function of the compressive strength.

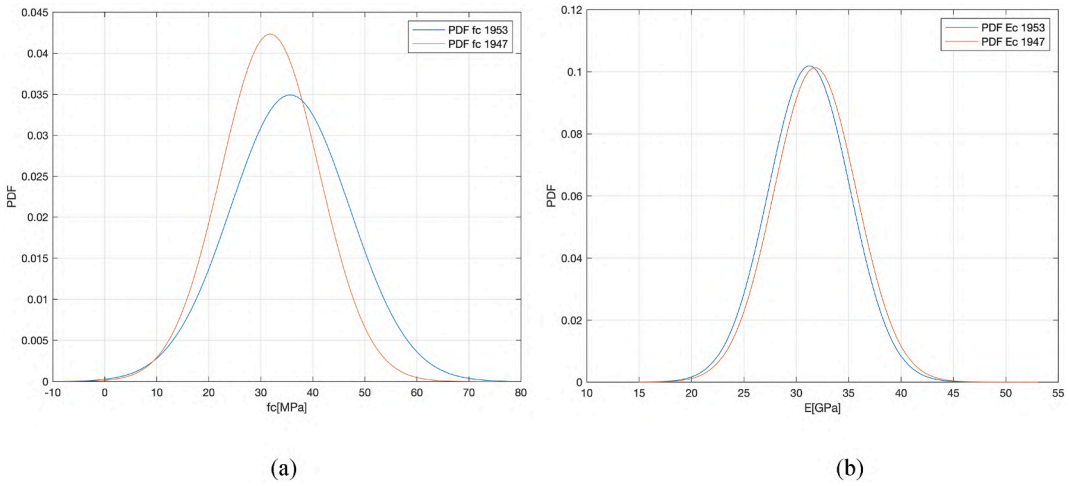


Fig. 4. Comparison of the two different time periods in terms of compressive strength (a) and Young Modulus (b).

structural integrity. In addition, these methods are highly valued in heritage settings due to their non-invasive and non-destructive nature. Previous research by [42], highlighted that the main challenges with the seismic response of the hall are related to the large number of structural elements that govern the dynamic behavior of the structures, that could be divided in macro-elements. These elements can be categorized into macro-elements, with the most critical responses associated with the undulated shell vault, out-of-plane tympanum movements, and the apse interacting with the main hall body. A preliminary finite element (FE) model of the

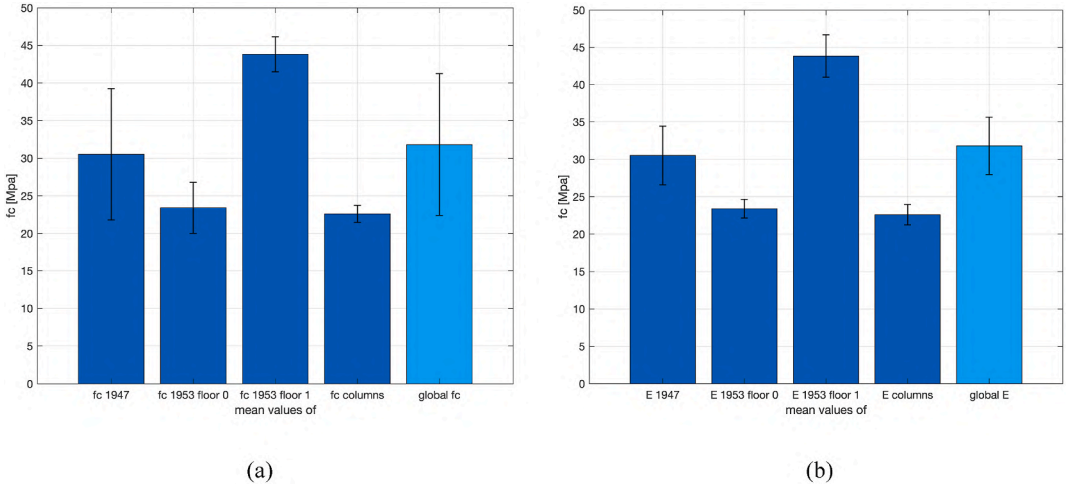


Fig. 5. Mean values of the compressive strength (a) and mean values of elastic modulus (b), categorized for different time periods and locations. The global mean values of all the acquired experimental samples are reported in light blue.

hall was used to optimize the design of an acquisition setup for dynamic testing. This setup aimed to maximize the content of extractable information and the spatial visualization of the modes, aiming at reconstructing the global and local dynamic behavior of the hall. Dynamic testing was conducted on October 11th, 2021, using ambient vibration excitation from wind and traffic. Data acquisition lasted up to 1 h, using a sampling frequency of 512 Hz, with 34 single-axis piezoelectric accelerometers (PCB Piezotronics, sensitivities of 1 V/g and 10 V/g) positioned on the vault, apse, and rear tympanum. The single setup prioritized modal decoupling and captured responses in all three spatial directions. Fig. 6 illustrates the dynamic experimental setup.

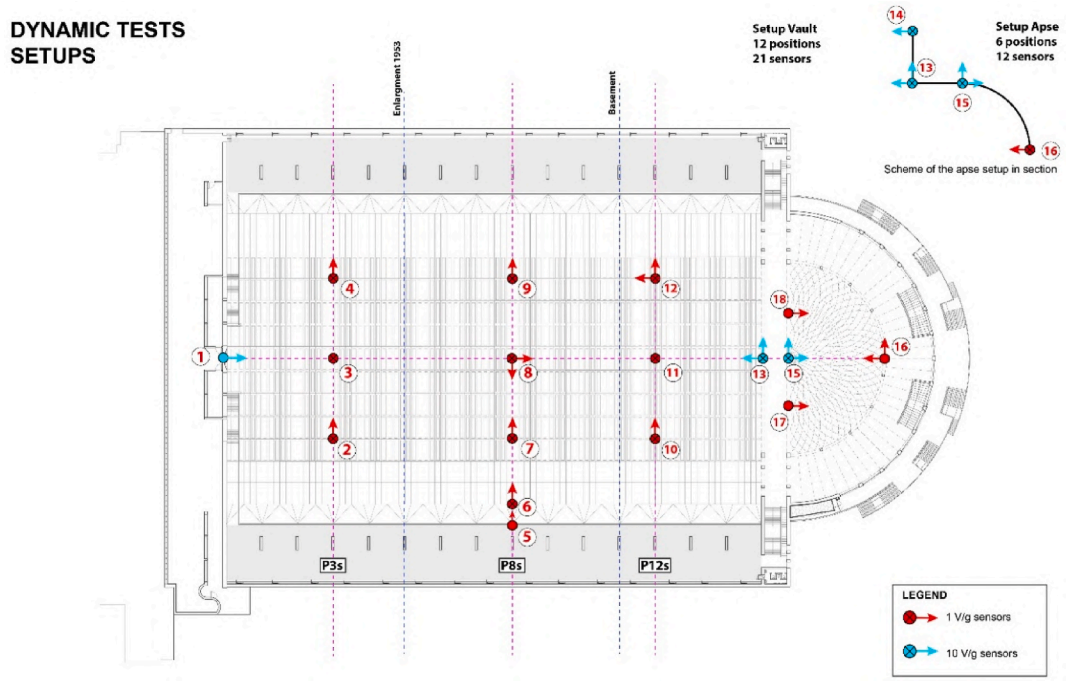


Fig. 6. Experimental setup installed on the structure; Sensor positions are indicated by circles, while acquisition directions are shown by red arrows. Vertical acquisition with a positive direction facing upwards is marked by cross 'x' within a red circle. Axes: x (transverse), y (longitudinal), z (vertical) [43].

3.3. Data processing

3.3.1. Mechanical testing

The data coming from the mechanical test were processed to infer some mechanical similarity in the structural components of the building, in order to reduce the number of material clusters to be used in the subsequent digitalization of the structural system. To achieve this purpose, a statistical analysis was performed to determine whether the tested cores extracted from the pillars corresponded to a unique material. Given the limited number of cores, the two sample T-test was deemed appropriate for this work. The test was conducted at a significance level of 5 % on the elastic modulus results (since density has low experimental variability), and was performed for each distinction criteria reported hereinafter.

- Part within the pillar system: pillar (P) or beam (B).
- The location of the pillar: north (n) or south (s) of the building.
- The construction process of the pillars: different levels (−1, 0 or +1).
- The construction time of the pillar: before (old) or after (new) the expansion of the building.

Table 2 shows the material clusters identified and their mean elastic modulus from core tests. Several clusters have only one test result, which is insufficient for proper analysis. As a result, these clusters were combined based on the distinction criteria established for the T-test, nevertheless, making a critical comparison of the results first.

The first test focuses on the differences between the mechanical characteristics of beam and column elements situated on the same level. The null hypothesis assumes that the actual average difference between the beams and pillars on a given level is negligible. The outcomes are presented in Table 3 for cores of the +1 level, south sidel. In the table, a value of one indicates that the hypothesis is true, while a value of zero implies that the null hypothesis is incorrect.

The results indicated that the material properties of beams and pillars within the same levels were not statistically different. Therefore, they were merged into a unique cluster, as well as the clusters with a single test result, as indicated earlier. Several considerations can be performed for the other distinction criteria, for which the only results are reported hereinafter.

- Location of the pillar: there are no significant differences in the elastic moduli between the northern and southern sides of the building, therefore these layers were merged.
- Construction process of the pillar: significant difference of the materials involved in the study.
- Construction time of the pillar: significant difference of the materials involved in the study.

The final material clusters obtained from the core testing are presented in Table 4.

3.3.2. Vibration-based testing

To ensure accurate identification, all the 34 signals were checked thoroughly to eliminate any records with anomalous behavior and no anomalies were detected. The signals were first adjusted to a global reference system to avoid mistakes in the eigenvector sign estimate. Then, they were processed to eliminate unwanted frequency components and trends. To achieve this, a constant detrend was applied, and a Butterworth filter with an order of four and cut-off frequencies of 1 and 15 Hz was used. The sampling frequency of the records was 256 Hz, which was reduced by a factor of two from 512 Hz to reduce noise and speed up the analysis. Lastly, both the Fourier and Welch spectrum were carefully analyzed with the peak picking method, in order to select potential candidate modes in the frequency domain. The analyzed signals, $s(t)$, lasted 1 h, which provided a particularly good frequency resolution of 5.2394e-04 [Hz].

Following the signal processing phase, the system identification was carried out. Due to the long duration of the signals, they were divided into four parts, and each sub-part was subjected to the SSI-CVA algorithm. The outcomes of the four sub-parts were then clustered and averaged to obtain unique estimates of each modal parameter. To ensure reliable and robust results, the order of the system varied between 270 and 430, and a stabilization analysis was performed to allow modes with estimated damping ratio between

Table 2
Identified material clusters from the core test results.

Layer	Mean E [MPa]	# of tests
Columns	27886.29	2
Level -1n_P_old	33804.35	1
Level 0s_P_old	34337.72	2
Level 0n_P_old	32922.18	2
Level +1s_B_old	32476.91	2
Level +1s_P_old	32118.19	2
Level +1n_B_old	32854.70	2
Level +1n_P_old	31005.08	2
Level 0s_P_new	28506.69	1
Level 0n_P_new	26750.79	1
Level +1s_B_new	36784.01	1
Level +1s_P_new	31233.75	1
Level +1n_P_new	32954.22	1

Table 3
T-student test results, for cores of the +1 level, south sidel.

T-STUDENT					
α = 0.05			**Layer**	Level +1s_B_old	Level +1s_P_old
			# of tests	2	2
			Mean Young's modulus [MPa]	32476.91	32118.19
Layer	**# of tests**	**Mean Young's modulus [MPa]**	**Standard deviation of Young's modulus [MPa]**	1867.91	634.47
Level +1s_B_old	2	32476.91	1867.91	1.00	1.00
Level +1s_P_old	2	32118.19	634.47	1.00	1.00

Table 4
Final material clusters and corresponding elastic moduli, and densities.

Elements	# of tests	Mean Young's modulus [MPa]	Standard deviation of Young's modulus [MPa]	Mean density [kg/m^3]	Standard deviation of density [kg/m^3]
Columns	2	27886	1368	2262	9
Old part	13	32710	3805	2362	58
New part, 0 floor	2	27629	1242	2395	77
New part, +1 floor	3	33657	2841	2363	19

0.1 % and 8 %. In addition to the stabilization study, a cluster analysis was implemented. The reference value of the frequency and damping used as the outcome of the overall identification procedure was assumed to be the average value of the frequency-damping cluster. To strengthen the results, the cluster analysis focused only on modes with a natural frequency in the range of 1.5–10 [Hz], after previously checking with preliminary identification for the absence of modes for frequencies below 1.5 [Hz], and the absence of relevant modes for the dynamic of the hall for frequencies over 10 [Hz].

Table 5 and Fig. 7 report the results of the identification in terms of natural frequency and main mode shapes of the first seven identified modes (for brevity reasons). It is important to highlight that mode 5 and 6 are local modes acquired by the sensor located on the tympanum in longitudinal direction (position #1 in Fig. 6).

4. Digital twinning

In the present section the definition, verification and validation of the numerical model supporting the experimental results is introduced.

4.1. The baseline model

The geometry of the hall was defined based on a geometrical survey performed by the *Dipartimento di Architettura e Design - DAD* of the *Politecnico di Torino* [36,37] and Nervi's original drawings of the design of the building [44]. After defining all the geometrical aspects of the hall, including sections of the elements, the Finite Element (FE) model of the structure was constructed. In this step, labels were created by grouping elements with specific properties, specifically, element type, section geometry, material, and location of the element. For the construction of the FE model, the hall was divided into its macro elements, namely: the undulated roof, the fanned elements, the inclined pillars, the half dome and apse, the back tympanum, the front tympanum, and the underground level. Fig. 8 reports the generated digital models.

The model is fully restrained at its base, it counts 202′522 elements for a total number of 510′462 Degrees of Freedom (DoFs) and an average mesh size of 1.5 m. As regards the mechanical parameters, they were initialized based on both mechanical tests (see Section 3), and average values from literature. About this, Table 6 reports the literature study for the definition of the mechanical parameters

Table 5
Results of the identification in terms of natural frequency and mode shapes of the first four identified modes. **The interpretation of description is based on the mode shapes of a simply supported beam with edge hinges.*

Mode	Nat. freq. [Hz]	Description*
1	1.70	Mode of the vault: 1st flex. mode in Y and 2nd flex. mode in X
2	1.94	Mode of the vault: 2nd flex. mode in Y and 2nd flex. mode in X
3	2.19	Mode of the vault: 3rd flex. mode in Y and 2nd flex. mode in X
4	2.48	Mode of the vault: 1st flex. mode in Y and 3rd flex. mode in X
5	2.85	Longitudinal response
6	2.89	Longitudinal response
7	3.24	Mode of the vault: 2nd flex. mode in Y and 3rd flex. mode in X

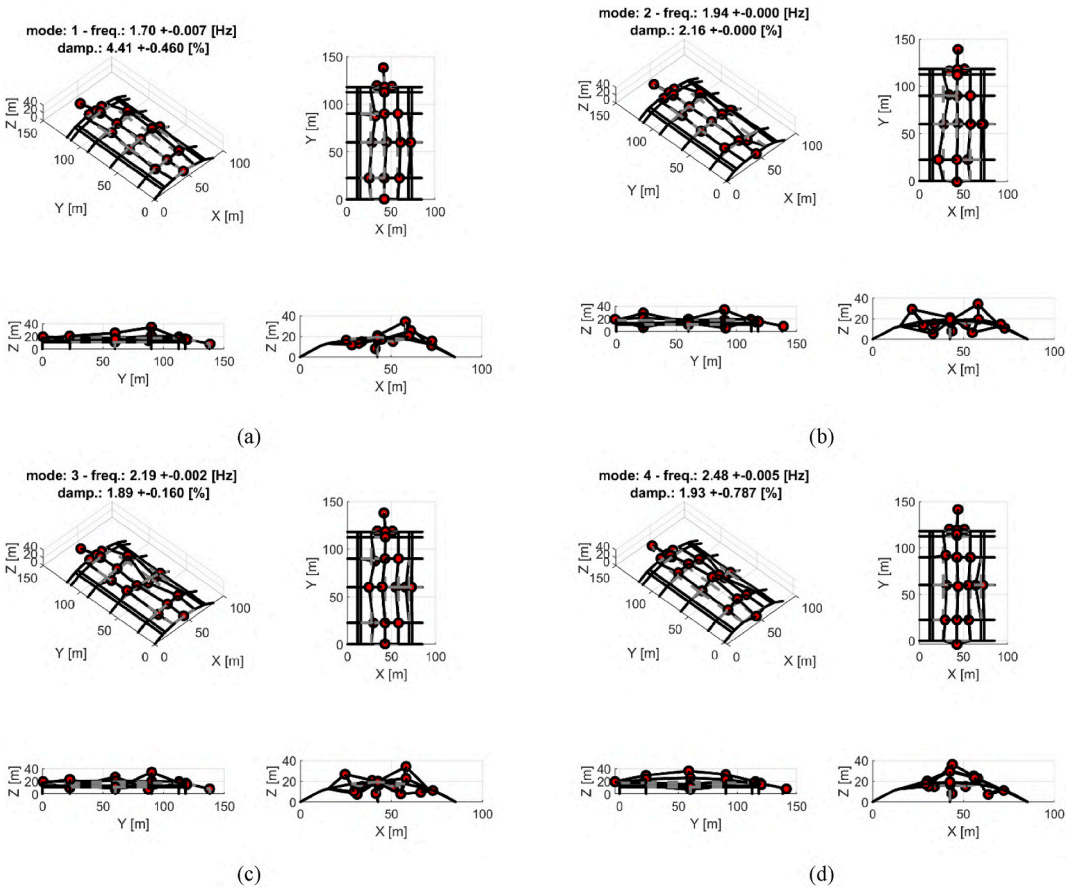


Fig. 7. Identified modes; (a) 1st mode; (b) 2nd mode; (c) 3rd mode; (d) 4th mode. The red spheres indicate the position of the sensors installed on the structure [43].

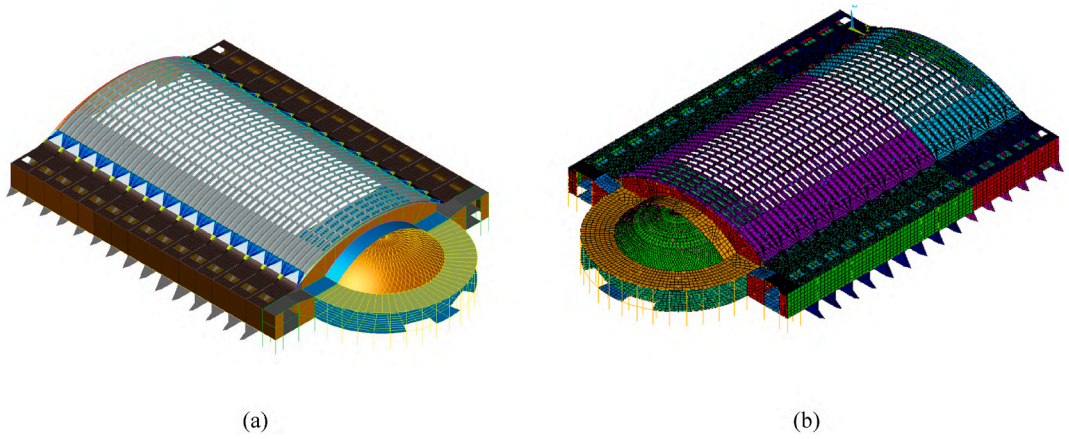


Fig. 8. Digital model of the Hall B: (a) geometrical model; (b) mechanical model.

value not associated to any mechanical test, specifically, in the table, E denotes the Young's modulus, ν the Poisson ratio, and ρ the density of the material. Instead, in Table 7, the parameters initialized with values obtained from the processing of mechanical tests data are reported.

Table 6
Literature-based defined parameters.

Description	ID number	Property	Value	Definition criteria
Ferrocement	1, 2, 6	E [GPa]	26	Based on a previous model realized on the same structure [42].
		ν [−]	0.2	Based on a previous model realized on the same structure [42].
		ρ [kg/m^3]	2500	Based on a previous model realized on the same structure [42].
Reinforced concrete	3, 4, 5, 16	E [GPa]	30	Common elastic modulus for concrete. Provided also by the Italian regulations[45], for a C25/30 concrete.
		ν [−]	0.2	Common Poisson ratio for concrete. Provided also by the Italian regulations [45].
		ρ [kg/m^3]	2500	Common density of reinforced concrete.
SAP20 + 4 mortar	10, 11	E [GPa]	21	Developed in a later section. Elastic modulus of the homogenized section with the slab concrete as reference, which is based on a previous model realized on the same structure [42].
		ν [−]	0.2	Poisson' ratio for the slab based on a previous model realized on the same structure [42].
		ρ [kg/m^3]	0	Developed in a later section. Equivalent density considering a mortar density of 2500 kg/m^3 [46].
SAP20 + 4 top slab concrete	12, 13	E [GPa]	21	Based on a previous model realized on the same structure [42].
		ν [−]	0.2	Based on a previous model realized on the same structure [42].
		ρ [kg/m^3]	6875	Developed in a later section, equivalent density considering the weight of the SAP system (https://www.leca.it/wp-content/uploads/2020/07/Guida-tecnica-consolidamento-solai.pdf).
Infill walls	14, 17	E [GPa]	2	Based on a previous model realized on the same structure [42], and supported by other sources, namely [47,48], which based on experimental test computed values around 20 GPa
		ν [−]	0.3	Some sources such, as [49,50], indicate that regulations [45] recommend a value of 0.25. On the other hand [46] computed a value of 0.32, therefore a value of 0.3 was assumed.
		ρ [kg/m^3]	1100	Developed in a later section. Equivalent density considering a mortar density of 2500 kg/m^3 [46].
SAP16 + 4 equivalent material (for shells)	15	E [GPa]	21	Developed in a later section. Elastic modulus of the homogenized section with the slab concrete as reference, which is based on a previous model realized on the same structure [42].
		ν [−]	0.2	Poisson' ratio for the slab based on a previous model realized on the same structure [42].
		ρ [kg/m^3]	764	Developed in a later section. Equivalent density considering the weight of the SAP system (https://www.leca.it/wp-content/uploads/2020/07/Guida-tecnica-consolidamento-solai.pdf).
SAP20 + 4 equivalent material (for shells)	18	E [GPa]	21	Developed in a later section. Elastic modulus of the homogenized section with the slab concrete as reference, which is based on a previous model realized on the same structure [42].
		ν [−]	0.2	Poisson' ratio for the slab based on a previous model realized on the same structure [42].
		ρ [kg/m^3]	1546	Developed in a later section. Equivalent density considering the weight of the SAP system (https://www.leca.it/wp-content/uploads/2020/07/Guida-tecnica-consolidamento-solai.pdf).
Slab reinforced concrete	22, 23	E [GPa]	21	Based on a previous model realized on the same structure [42].
		ν [−]	0.2	Poisson' ratio for the slab based on a previous model realized on the same structure [42].
		ρ [kg/m^3]	2500	Common density of reinforced concrete.

4.2. Model verification

In the present section the verification of the numerical model is performed thorough a gravity load analysis and an eigen-analysis. The numerical simulations were carried out in the ANSYS [51] environment, while the analysis and processing of results were performed through a custom MATLAB routine [52]. The procedure operated via batch processing, allowing automatic interaction between the finite element model and the numerical algorithms.

4.2.1. Debugging with gravity load analysis

To debug the FE model, a static analysis is performed, where the hall's response is studied by considering only the elements' self-weight. The analysis indicate that the hall experiences its maximum deformation around the center of the roof, particularly at the fanned elements and pillar head, while these elements undergo much lower deformation near the tympanums. The maximum displacement value is approximately 0.0235 m.

4.2.2. Debugging with eigen-analysis

Due to the size of the model (510′462 Dofs), the numerical analysis generated a large number of solutions to the eigenvalue

Table 7
Material component of the numerical model.

ID number	Description	Model parameters: E [GPa], ν [−], ρ [kg/m^3]
1	Roof ferrocement (new)	See Table 6
2	Roof ferrocement (old)	See Table 6
3	Roof concrete (new)	See Table 6
4	Roof concrete (old)	See Table 6
5	Cupule concrete (old)	See Table 6
6	Cupule ferrocement	See Table 6
7	Back part concrete (old)	27.89, 0.2, 2262
8	Pillar floor +1 concrete (new)	33.66, 0.2, 2363
9	Pillar floor +1 concrete (old)	32.71, 0.2, 2362
10	SAP 20 + 4 beam (new)	See Table 6
11	SAP 20 + 4 beam (old)	See Table 6
12	SAP 20 + 4 top slab concrete (new)	See Table 6
13	SAP 20 + 4 top slab concrete (old)	See Table 6
14	Infill (old)	See Table 6
15	SAP 16 + 4 equivalent material (for shells)	See Table 6
16	Front part concrete (new)	See Table 6
17	Infill (new)	See Table 6
18	SAP20 + 4 equivalent material (for shells)	See Table 6
19	Pillar floor 0 and -1 concrete (new)	27.30, 0.2, 2395
20	Pillar floor 0 concrete (old)	32.71, 0.2, 2362
21	Pillar floor −1 concrete (old)	32.71, 0.2, 2362
22	Slab concrete old	See Table 6
23	Slab concrete new	See Table 6

problem. However, this is not consistent with reality, and most solutions are only numerical. Additionally, the structure is comprised of many elements; thus, while certain modes may seem incoherent when considering the whole building, they might accurately represent the behavior of specific elements of the hall. Therefore, a careful analysis was carried out to identify vibration modes that are consistent from both a global and a local perspective, thereby enabling a well-developed description of the dynamic response of the structure. Experimentally, it was observed that the frequency content of the building reach up to approximately 10 [Hz]. As a result, 300 modes were computed to achieve those values of natural frequency. Then, each mode was individually assessed in order to identify the ones that appeared reasonable and consistent with experimental observation.

- The numeric modes 1, 4, 5, and 9 are the modes that excite the most mass. Both modes 1 (Fig. 9 (a)) and 9 exhibit a high translational behavior in the transverse direction.
- With regard to the z direction, numeric mode 2 stands out from the rest, with a high mass participation factor and a high vertical displacement in the center of the undulated vaults, as seen in Fig. 9 (b).

4.3. Sensitivity analysis

A sensitivity analysis of structural simulator can be used to determine which model parameters are the most important and most likely to affect system behavior in terms of some model properties (e.g., natural frequencies). Following a sensitivity analysis, the knowledge of critical parameters must be deepened, whereas parameters with a negligible effect can be ignored. In this sense,

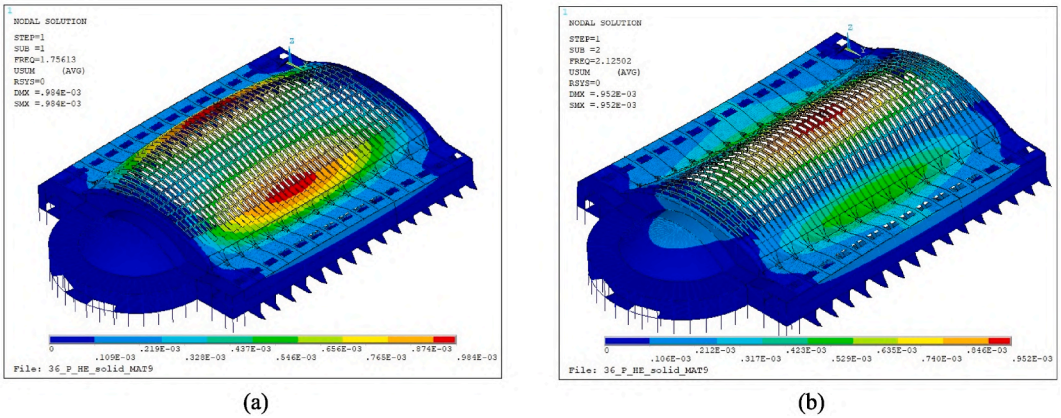


Fig. 9. Deformed shape of numeric mode 1 (a), and 2 (b).

sensitivity analysis plays a role in reducing the computational burden of the validation process, which in many cases would be insurmountable. The FE model consists of 23 materials and 69 material elastic properties. The sensitivity was performed thus performed considering 70 parameters; the 69 material properties plus an addition parameter that regulate the stiffness (Young's modulus) of the pillar head, in order to consider different internal constrain degrees. The procedure consists in changing, for each parameter P_i, its value with a small increments ΔP_i within predefined limits $P_{i.min}$ and $P_{i.max}$ and performing an eigenvalue analysis to obtain the variation in the structure's vibration natural frequencies due to these parameter changes. A literature review (see Table 6) was conducted that focused mainly on studies involving material tests in order to understand reasonable ranges for the parameters used in the FE model. The considered ranges and step increments for the different materials of the FE model are presented in Table 8. Parameter bounds in Table 8 were set using statistical variability from core tests (Table 1) when available; for other materials, bounds were inferred from analogous structural components with added conservative margins to encompass modeling uncertainties. Then, increment sizes (ΔE, $\Delta\nu$, Δρ) were determined via preliminary parametric studies to ensure each step induced negligible modal variation, thereby preserving sensitivity resolution.

Sensitivity analysis employed a local *one-at-a-time* strategy to manage computational cost. For each parameter, 30 uniformly spaced samples were drawn within the defined bounds, yielding 2160 total eigen-analyses. Variance-based sensitivity metrics were then computed per each mode to quantify each parameter influence. This approach was also chosen given the prior experimental knowledge available about the nominal values of the mechanical parameters, avoiding high-dimensional sampling, and ensuring unbiased sensitivity estimates (i.e. uniform sampling) while preserving computational efficiency.

The numerical analysis generates a large number of vibration modes. However, not all these modes are coherent with the building's actual behavior (e.g., numerical artifacts generated by the model discretization). In addition, for computational efficiency, only the most relevant modes were considered for the analysis, specifically those that were significant to the hall and roof response from a global perspective. To this end, it was observed that from the numeric mode of vibration 15 the deformed shape began to show a large number of local modes, characterized by little participating mass, so the sensitivity was restricted to the first 15 modes. The results of the analysis provide a set of vibration natural frequencies for each of the selected 15 modes, *m,* at every value increment of each of the 70 parameters, *i*. The sensitivity is then measured by means of the variance σ^2_{im} of the natural frequencies over the parameter space, which is normalized to the total variance (i.e., $\sum_{i,m}\sigma^2_{im}\Big)$ to obtain the fraction of variance r_{im}, used to estimate the influence of the parameters on each computed mode. Equation (1) reports the calculated fraction of variance.

$$r_{im} = \frac{\sigma^2_{im}}{\sum_{i,m}\sigma^2_{im}} \tag{1}$$

4.4. Model validation

This subsection focuses on the model validation of the Hall B structure. The model validation relies on three main points.

Table 8
Elastic moduli, Poison's ratio, and densities range definition. *Sensitivity evaluated through the equivalent density applied to material 12. ** Sensitivity evaluated through the equivalent density applied to material 13.

Mat. ID	Range E [Pa]		ΔE [Gpa]	Range ν [−]		Δν [−]	Range ρ [kg/m^3]		Δρ [kg/m^3]
1	5.00E+09	3.00E+10	8.33E-01	0	0.25	8.33E-03	1800	3000	26.67
2	5.00E+09	3.00E+10	8.33E-01	0	0.25	8.33E-03	1800	3000	26.67
3	2.00E+10	4.50E+10	8.33E-01	0	0.25	8.33E-03	2100	2600	16.67
4	2.00E+10	4.50E+10	8.33E-01	0	0.25	8.33E-03	2100	2600	16.67
5	2.00E+10	4.50E+10	8.33E-01	0	0.25	8.33E-03	2100	2600	16.67
6	5.00E+09	3.00E+10	8.33E-01	0	0.25	8.33E-03	1800	2600	26.67
7	2.30E+10	3.50E+10	4.00E-01	0	0.25	8.33E-03	2150	2550	13.33
8	2.50E+10	4.30E+10	6.00E-01	0	0.25	8.33E-03	2250	2500	8.33
9	2.10E+10	4.45E+10	7.83E-01	0	0.25	8.33E-03	2150	2550	13.33
10	1.50E+10	3.00E+10	5.00E-01	0	0.25	8.33E-03	6675*	6925*	8.33
11	1.50E+10	3.00E+10	5.00E-01	0	0.25	8.33E-03	6675**	6925**	8.33
12	1.50E+10	3.00E+10	5.00E-01	0	0.25	8.33E-03	6475	6975	16.67
13	1.50E+10	3.00E+10	5.00E-01	0	0.25	8.33E-03	6475	6975	16.67
14	1.00E+09	3.00E+09	6.67E-02	0	0.4	1.33E-02	700	1300	20.00
15	1.50E+10	3.00E+10	5.00E-01	0	0.25	8.33E-03	1260	1380	4.00
16	2.00E+10	4.50E+10	8.33E-01	0	0.25	8.33E-03	2100	2600	16.67
17	1.00E+09	3.00E+09	6.67E-02	0	0.4	1.33E-02	700	1300	20.00
18	1.50E+10	3.00E+10	5.00E-01	0	0.25	8.33E-03	1410	1580	5.67
19	2.30E+10	4.30E+10	6.67E-01	0	0.25	8.33E-03	2150	2650	16.67
20	2.10E+10	4.45E+10	7.83E-01	0	0.25	8.33E-03	2150	2550	13.33
21	2.10E+10	4.45E+10	7.83E-01	0	0.25	8.33E-03	2150	2550	13.33
22	1.50E+10	3.00E+10	5.00E-01	0	0.25	8.33E-03	2100	2600	16.67
23	1.50E+10	3.00E+10	5.00E-01	0	0.25	8.33E-03	2100	2600	16.67
24 (Pillar head)	2.10E+10	6.64E+10	1.51E+0	–	–	–	–	–	–

- A preliminary assessment of the digital model corroborated with experimental data directly estimated by mechanical test, when available.
- A mode matching analysis.
- The inverse search of optimal solutions for *variables input* and *calibrations input.*

The inverse searching of variables and calibrations input involves a recursive process where for each iteration predetermined inputs are modified within a specified range, and the model is run to calculate the objective function value to be minimized. Once optimal values are defined, the results include the updated parameter values, as well as correlated modes, error in frequency and error in mode shape. These results are useful to evaluate the validity and reliability of the updated system, and to investigate source of discrepancy that affect the model predictions.

4.4.1. Preliminary assessment

The preliminary assessment focuses on the comprehension of the conditions and limitations of the model is gained. The goal is to limit possible errors during the calibration phase, to help the algorithm towards a more accurate solution. Additionally, weaknesses can be identified and resolved before the calibration phase of the digital model. This is achieved by analyzing the correspondence between the experimental mode shapes and the numerical mode shapes coming from the model, in order to define the modes to be considered during the calibration. This task is the so-called mode coupling or mode matching. It can be performed by forcing the numerical modes to be coupled in ascending order to the experimental modes or not based on some specific metric. In this work the Modal Assurance Criterion (MAC) was averaged to the absolute normalized error in frequency (absolute difference between experimental and numerical natural frequency, normalized to the experimental value) to define the coupling degree. The result for the mode coupling is presented in Table 9.

In Table 9 it is observed that experimental modes 2 and 3 are well captured by the model, while the rest of the modes present high error values either in frequency, MAC or both. Regarding the error in MAC, for numeric mode 11 and higher its value increases suddenly with respect to the previous modes. This means that starting from mode 11, there is a high discrepancy in the experimental and numerical mode shapes. No conclusions can be drawn about these mode shapes, but it is evident that the model corroborated with mechanical test results is not able to capture them. Consequently, these modes are discarded for the model updating as they can contaminate the objective function, significantly increasing the overall error due to modes that cannot be captured by the model. Contrary, the model represents properly (considering that it is not calibrated yet) the first four experimental modes of the building in terms of mode shape, with their corresponding numerical modes being within the first seven modes for the not forced matching approach. The most significant issue is the mode inversion happening between numerical modes 7, 2, and 3 corresponding to the experimental modes 3 and 4, and 2 respectively. This explains the sudden increase in the numeric mode number in the case of forced matching. Mode inversions are related to different causes, such as lack of torsional stiffness and erroneous mass distribution, which are the likely reasons in this model. More in general, uncertainties on variable inputs usually are the cause of issues in modes. For the hall B, four sources of uncertainty have been identified.

- The unmodelled geometry of the complex that interacts with the Hall B. However, the modelling of these structures is out of the scope of this work and it is neglected for the validation phase.
- The stiffness of the infill walls: which is represented by their elastic modulus (*first variable input*). This property depends on factors such as cracks, connectivity with other elements, presence of holes, etc. However, establishing the state of these walls is not straightforward, so a high uncertainty is involved, making it difficult to set a value for this parameter.
- The weight of the undulated roof, which is considered in the model through the density of the roof elements, however, there is additional weight on the roof due to the roofing, pipes, etc. As reported in Section 5, during the sensitivity analysis it was observed that the density of the undulated roof has an important impact on the dynamic response of the structure, so an equivalent density (*second variable input*) should be considered for the undulated roof elements to account for this added weight.
- The degree of constraint of the undulated roof: which is determined by the connection between the pillar and the undulated roof. This uncertainty is controlled by the elastic modulus of the pillar head. Nonetheless in Section 5, the sensitivity analysis indicated that this parameter has low impact on the response of the hall, thus the analysis of this parameter is neglected for the validation phase.

Table 9
Results of the mode matching forcing (left side), and without forcing (right side) the coupling in ascending order.

Experimental mode	Matching numerical mode	Predicted frequency [Hz]	Error in frequency	MAC	Matching numerical mode	Predicted frequency [Hz]	Error in frequency	MAC
1	1	1.50	11.66 %	0.50	1	1.76	−3.55 %	0.46
2	2	1.81	6.85 %	0.73	3	2.30	−18.42 %	0.74
3	5	2.03	7.01 %	0.75	7	2.81	−28.48 %	0.68
4	23	3.06	−23.41 %	0.57	2	2.13	14.40 %	0.72
5	28	3.28	−14.99 %	0.14	11	3.29	−15.48 %	0.17
6	33	3.46	−20.26 %	0.11	16	3.86	−33.73 %	0.15
7	34	3.52	−8.88 %	0.21	16	3.86	−19.39 %	0.37

In order to address the issue of the mode inversion, before to proceed with the model validation trough model updating, a study aimed at defining the value of some variable inputs is carried out in Section 5.

4.4.2. Mode matching

To define a correct matching between the experimental outcomes and the numerical predictions, the experimental mode shapes were interpolated by the FE method, forcing the experimental mode shapes coordinates to the FE model. The results of the matching are shown in Fig. 10 for five of the seven identified modes. Indeed, no correspondence was identified for experimental modes 5 and 6 with enough certainty to be considered in the validation phase (even if a discrete match in the mode shapes of experimental modes 5 and 6 is found with numeric modes 4 and 5, contemplating the local modes of the front tympanum and the longitudinal response). The results of the mode matching in terms of natural frequencies is reported hereinafter.

- Experimental mode 1 of 1.70 Hz corresponds to the numeric mode 1 with a frequency of 1.76 Hz.

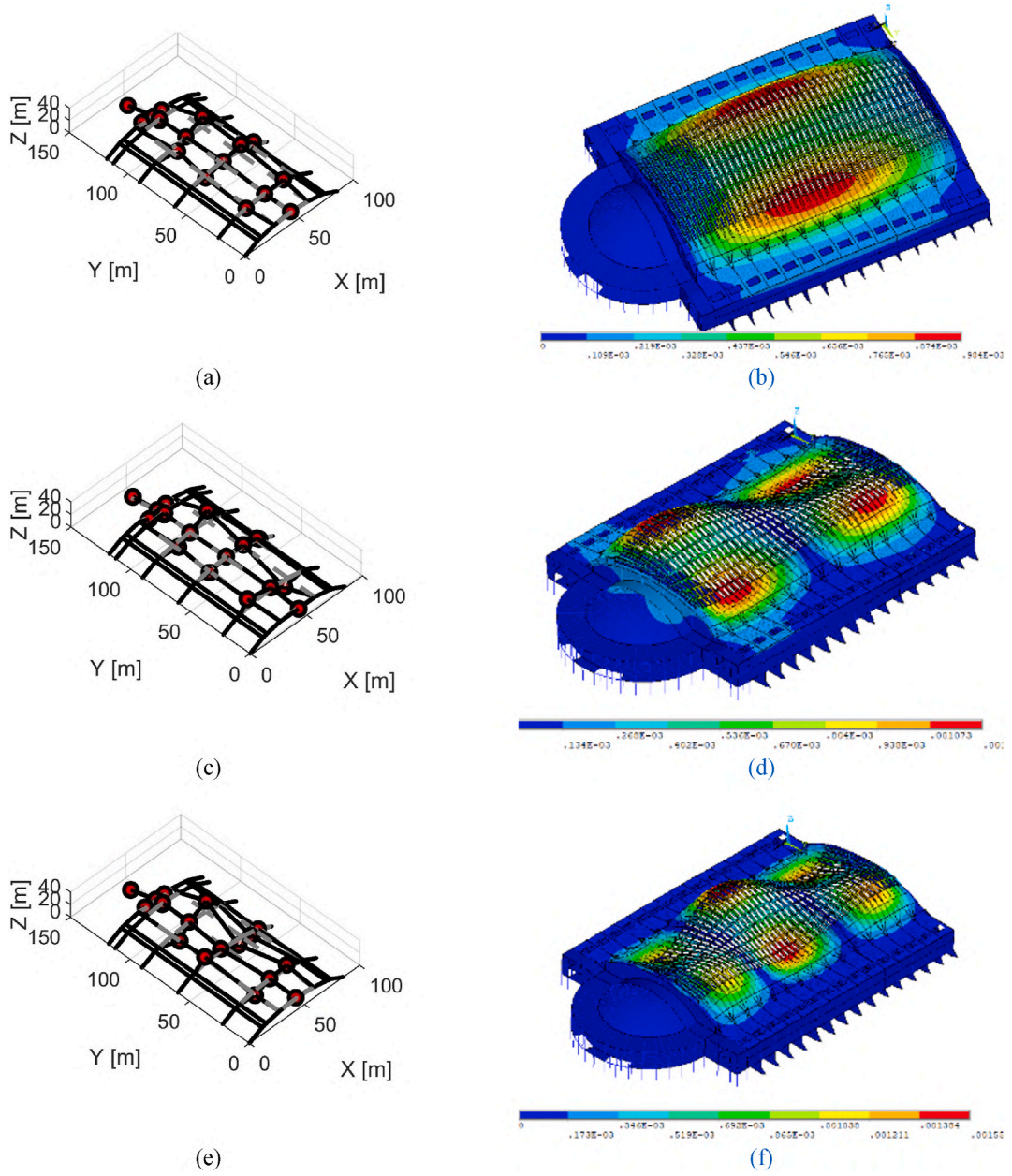


Fig. 10. Experimental and numerical mode shape of mode 1 (a) and (b). Experimental mode 2 (c) and numeric mode 3 (d). Experimental mode 3 (e) and numeric mode 7 (f). Experimental mode 4 (g) and numeric mode 2 (h). Experimental mode 7 (i) and numeric mode 6 (j).

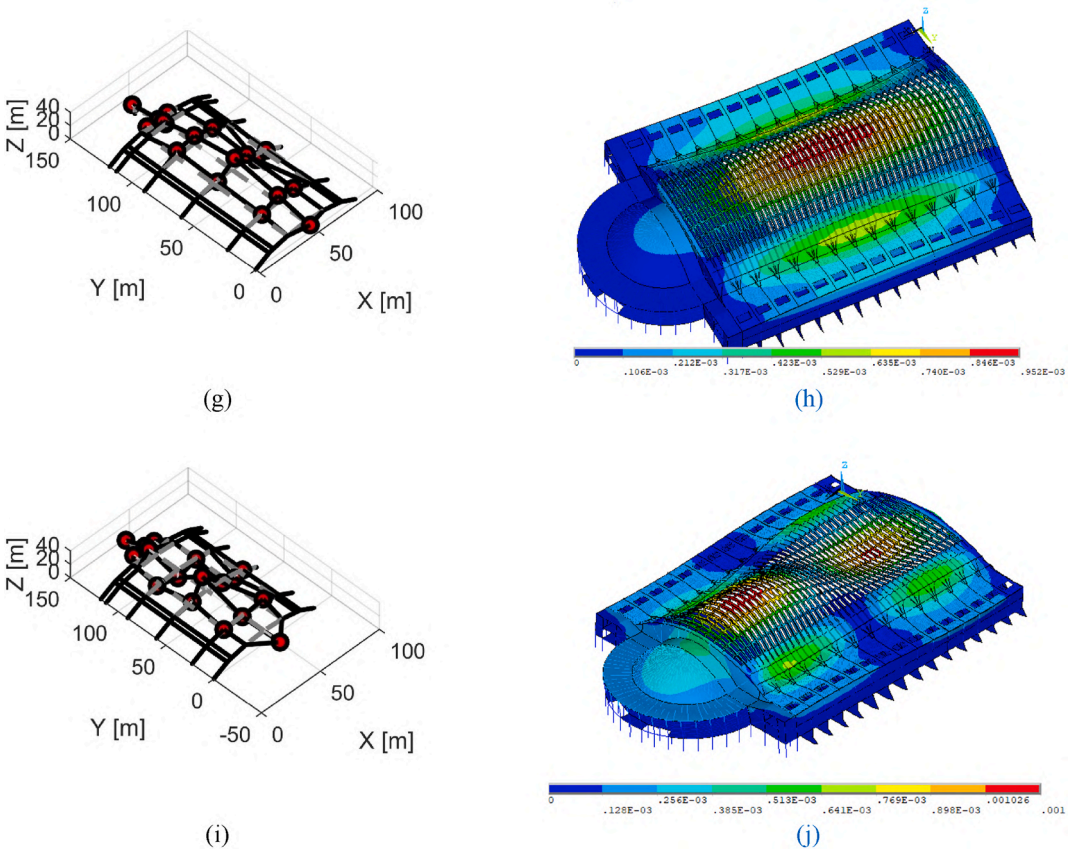


Fig. 10. (*continued*).

- Experimental mode 2 of 1.94 Hz corresponds to the numeric mode 3 with a frequency of 2.30 Hz.
- Experimental mode 3 of 2.19 Hz corresponds to the numeric mode 7 with a frequency of 2.81 Hz.
- Experimental mode 4 of 2.48 Hz corresponds to the numeric mode 2 with a frequency of 2.13 Hz.
- Experimental mode 7 of 3.24 Hz corresponds to the numeric mode 6 with a frequency of 2.70 Hz.

Thus, all the first four experimental modes follow the automatic matching approach without forcing the coupling in ascending order, instead, as regard the experimental mode 7, the automatic matching failed to capture the experimental mode shape, which was actually represented by the sixth numeric mode instead of mode 16 (see Table 9).

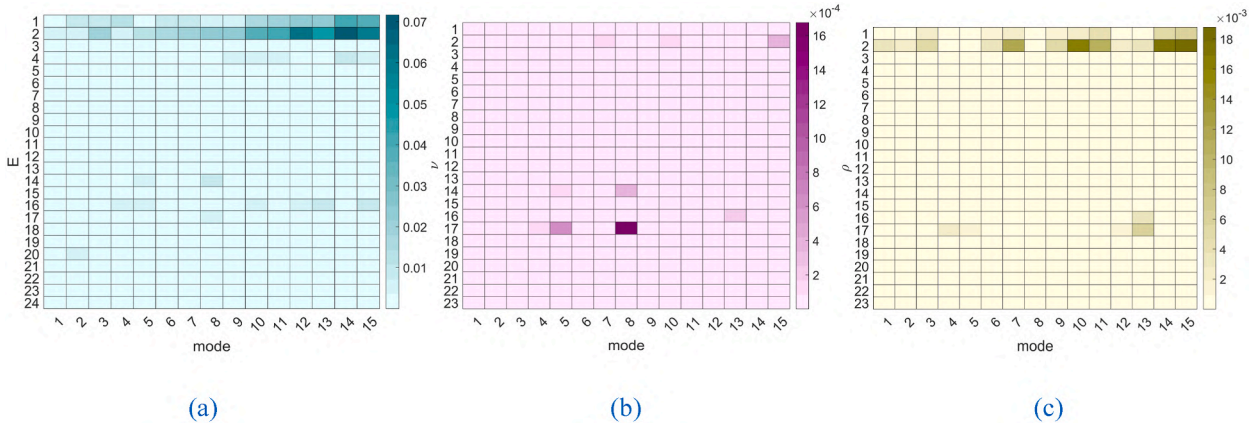


Fig. 11. Sensitivity analysis results in terms of elastic modulus (a), Poisson rations (b), and densities (c) of the model materials.

5. Discussion of the results

In this section the results of the sensitivity analysis and the model validation are critically analyzed and discussed.

5.1. Sensitivity analysis

The sensitivity analysis aimed at identifying what mechanical parameter affects most a specific vibration mode, in terms of natural frequency variation. This can be visually represented by a bidimensional heatmap (Fig. 11). In particular, in the figure, the fraction of variance (see Equation (1)) for the first numerical 15 modes has been reported for the Young's moduli, Poisson rations, and densities of the model materials.

Although the previous graph may be difficult to analyze, some conclusions can be drawn. It is evident that the elastic modulus of the first two materials (new roof ferrocement and old roof ferrocement, respectively) and the elastic modulus of the infill walls have by far the biggest impact on the building's dynamic behavior. Moreover, the Poison's ratios represent a negligible influence on the vibration modes. These results require to be further processed to draw more definitive conclusions. In particular, understanding which parameter have the greatest influence on specific modes can provide the path to choose the properties needed for the validation phase. This can be done by analyzing the fraction of variance independently for each mode of vibration and detecting the most sensitive parameters accordingly. The results are reported hereinafter for the first seven modes and the three main parameters that affect each mode (see Table 7 for the ID number).

- First mode: E_2, E_{20}, ρ_2
- Second mode: E_1, E_2, E_{20}
- Third mode: E_1, E_2, ρ_2
- Fourth mode: E_1, E_{16}, E_2
- Fifth mode: E_2, E_{14}, E_{16}
- Sixth mode: E_1, E_2, ρ_2
- Seventh mode: E_1, E_2, ρ_2

From this more in-depth analysis emerged that for the density, only the value of the roof ferrocement material was significant in the analysis, while the remaining material densities have demonstrated to be irrelevant. The most influencing material properties for the Hall B are summarized in Table 10.

5.2. Model validation

In this section the validation through the model calibration task is performed. It is important to preface that the calibration was deliberately confined to experimental vibration modes 1, 2 and 3 and their associated roof stiffness and density parameters, as the variance-based sensitivity analysis identified these modes and variables as responsible for over 75 % of the total modal variance and as critical to the global dynamic response. Higher-order modes exhibited low mass participation factors and inconsistent MAC values, so they were excluded to prevent contamination of the objective function. This selection reduced problem dimensionality, improving convergence speed (efficiency) and robustness of the analysis.

5.2.1. Setting of the variable inputs values

Before the *calibration inputs* updating, the *variable inputs* (i.e., E_{14} and ρ_2) calibration should be independently performed in order to reduce the propagation of the uncertainty of these parameters during the optimization phase; thus, corrupting the results of the model updating. The defined ranges of variation for the *variable inputs* are reported in Table 11. Since E_{17} and ρ_1 are associated to the same structural elements to which E_{14} and ρ_2 are associated (but referring to the new part of the pavilion), they were included in the definition of the variable inputs value. To perform the *variable inputs* updating, just the vibrational modes of the vault were considered, i.e., mode 1, 2, 3, 4, and 7, being mode 5 and 6 associated to the local behavior of the tympanum and less representative of the global behavior of the system.

The lower limit of the densities is defined from the sensitivity analysis, which corresponds to the density of cement mortar. The upper limit is defined in a way to consider the presence of many non-structural elements increasing the weight of the roof. On the other hand, for the lower limit of the infill walls elastic moduli, a very low value is set to consider an almost null interaction with the main structure. The upper value, instead, is defined as the upper limit given by the Italian regulations [45]. With the parameter ranges defined, the algorithm was run. The result, in terms of mechanical parameter values, obtained is reported Table 11. It is evident that the updated densities have much greater value than the initial ones, which is reasonable, as the initial value considers only the ferrocement material. On the other hand, the infill walls also undergo an increase of their stiffness with respect to their initial values, being the old part of the hall the most impacted. The final elastic moduli of the infill walls are within the range given for this typology according to the Italian regulations. Although this may seem counterintuitive, the updating was conducted considering modes which are focused on the undulated roof, therefore, it does not necessarily represent the actual conditions of the infill walls, but it is rather a numerical result which seeks to optimize the model capacity in capturing and replicating the undulated roof's response.

Table 10
Most influencing material properties. *Variable inputs.

Property ID	Description
E_1	Elastic modulus of the roof ferrocement (new part)
E_2	Elastic modulus of the roof ferrocement (old part)
E_{14}*	Elastic modulus of the infills (old part)
E_{16}	Elastic modulus of the front part concrete (new part)
E_{20}	Elastic modulus of the pillar concrete at floor 0 (old part)
ρ_2*	Density of the roof ferrocement (old part)

Table 11
Variable inputs, their calibration range, and results of the variable inputs updating.

Material property	Min Value	Max value	Initial value	Updated value
ρ_1	1800 [kg/m^3]	4500 [kg/m^3]	2500 [kg/m^3]	4282.9 [kg/m^3]
ρ_2	1800 [kg/m^3]	4500 [kg/m^3]	2500 [kg/m^3]	4363.7 [kg/m^3]
E_{14}	0.002 [GPa]	5.60 [GPa]	2.00 [GPa]	4.99 [GPa]
E_{17}	0.002 [GPa]	5.60 [GPa]	2.00 [GPa]	0.23 [GPa]

5.2.2. Calibration inputs updating

After the definition of the variable inputs values, the calibration inputs updating is performed. Although four parameters were defined to undergo updating in this subsection the scope has been narrowed down to the roof local modes. This decision is supported by the clear and demonstrated structural prominence of the roof and its substantial role in the dynamic response of the building. Consequently, the updating parameters have also been restricted to those corresponding to the roof to ensure consistent results, neglecting parameters that governs local behaviors of other components, i.e., E_{16}, which corresponds to the front tympanum concrete. Thus, the considered vibration modes were restricted to experimental vibration modes 1, 2 and 3, accordingly. Table 12 gives these parameters along with the considered range, and results of the updating.

Even though a meticulous study was performed to define the geometry of the model, there is an external factor that was not considered in the modelling, which is the presence of adjacent structures. The pavilion in fact is not isolated, and therefore some lateral stiffness is neglected in the analysis. This is consistent with the previously obtained results, as the mode inversion is seen in the modes that extend lateral, and where a variation in the lateral stiffness would have some effect, while the roof local modes (identified modes 1, 2 and 3) are predicted accurately and are not significantly influenced by an additional lateral stiffness. To solve the issue of mode inversion the adjacent hall A should be included in the model, but that goes beyond the scope of this work. Consequently, the model validation is conducted considering only the modes which are correctly captured by the model, specifically, experimental modes 1, 2 and 3, which are vibration modes of the undulated roof.

The updated roof's elastic moduli are presented in Table 12, which indicates a negligible change in the modulus of new part (E_1), but a substantial reduction of the modulus of the old part (E_2). Since the old part comprises most of the hall, a greater adjustment on E_2 to calibrate the model is coherent. Table 13 reports the corresponding numerical modes and errors. The model appears to effectively capture mode 2 and 3, with low frequency errors. However, mode 1 is weakly reproduced. The MAC values for the experimental modes 2 and 3 are within the previously defined thresholds, indicating that the model replicates the mode shapes correctly. However, mode 1 is not well reproduced by the model. A possible reason for the discrepancies regarding mode 1 is that its effects, although it is a roof local mode, extends laterally to the border structural elements, and to adjacent buildings that are not considered in the modelling of the pavilion.

To verify the predicted mode shapes, the numerical modes 1, 2 and 4 are displayed in Fig. 12. The resulting plots confirm the correctness of the mode shapes. Furthermore, the numerical inversion has been partially solved, with the updated model, correctly placing the first 2 modes.

The numerical modes 3 and 5 are also illustrated in Fig. 13 to understand if the model suffered some higher impact due to the model updating.

The accuracy of the FE model in replicating the mode shapes is evident, but their positioning is not. There is still an inversion between the numerical modes 3 and 4. While numerical mode 5 corresponds to experimental mode 7, indicating a misplacement. However, since experimental modes 5 and 6 are longitudinal modes, and the model has a weakness in replicating the hall's behavior in this direction, these discrepancies are not unexpected. Nevertheless, the updating was based solely on the undulated roof behavior, so these discrepancies just represent additional remarks about the updated model.

Table 12
Calibration inputs, their calibration range, and results of the calibration inputs updating.

Material property	Min Value [GPa]	Max value [GPa]	Initial value [GPa]	Updated value [GPa]
E_1	5	35	26	34.60
E_2	5	35	26	20.00
E_{20}	21	44.5	32.71	44.10

Table 13
Results of the model updating.

Experimental mode	Natural frequency [Hz]	Matching numerical mode	Predicted frequency [Hz]	Final error in frequency	Initial error in frequency	Final error in MAC	Initial error in MAC
1	1.70	1	1.546	8.82 %	9.36 %	51.46 %	52.88 %
2	1.94	2	1.917	1.32 %	−1.22 %	26.51 %	25.09 %
3	2.19	4	2.234	−2.10 %	−6.56 %	22.49 %	22.72 %

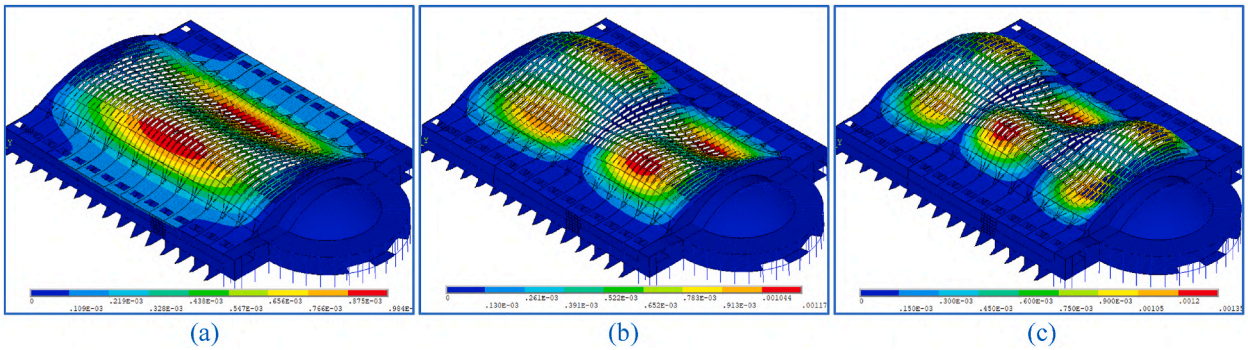


Fig. 12. Updated numerical mode 1, 2 and 4.

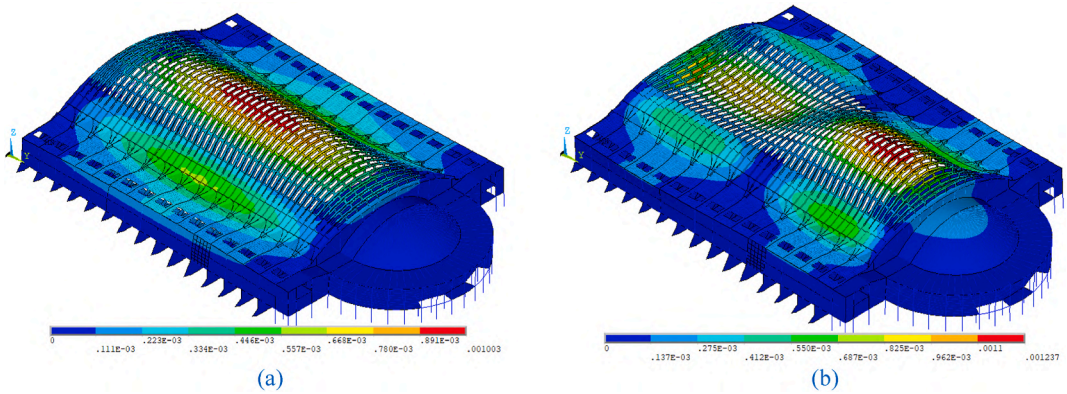


Fig. 13. Updated numerical mode 3 (a) and 5 (b).

To conclude, the final material parameter properties are illustrated Table 14, where the updated variable inputs are highlighted in light grey and the calibrated inputs in dark grey, while the results of the model validation procedure for the different step of analysis are reported in Fig. 14.

Despite significant improvements in mode alignment, modes 3 and 4 remain inverted due to persistent discrepancies linked to unmodeled structural interactions and local mass/stiffness uncertainties. In particular, the exclusion of adjacent building wings and assumptions on boundary conditions likely affect the modal coupling in that frequency range. To conclude, from Fig. 14 it is possible to notice that even if the procedure produced a slightly reduction of the natural frequency errors (between the experimental evidence and numerical prediction), the error in coupling was drastically reduced, producing a numerical configuration less affected by model discrepancy with respect to the initial model configuration, and thus more suitable for automatic model updating tasks.

6. Conclusions

Although there are many tools to detect a reversal of vibration modes, the automation of the correction of this problem is still an unsolved problem, which however is crucial to ensure that the model updating is accurate. If these inversions are not addressed, the updated model may not correctly represent the dynamic behavior of the structure, leading to inaccurate predictions and potentially poor engineering decisions. Addressing the vibration mode reversal problem requires careful analysis of modal data, the use of correlation metrics such as MAC, and an iterative process of model updating. This help to ensure that the predicted and experimental modes are correctly aligned, improving the accuracy of the updated model.

Table 14
Final material properties of the model. Highlighted in grey are the variable (light grey) and calibration (dark grey) inputs.

Material number	Description	E [Gpa]	ν [-]	ρ [kg/m^3]	ΔE [%]	Δρ [%]
1	Roof ferrocement (new)	34.60	0.2	4282.9	+33	+71
2	Roof ferrocement (old)	20.00	0.2	4363.7	-23	+74
3	Roof concrete (new)	30.00	0.2	2500	-	-
4	Roof concrete (old)	30.00	0.2	2500	-	-
5	Cupule concrete (old)	30.00	0.2	2500	-	-
6	Cupule ferrocement	26.00	0.2	2500	-	-
7	Back part concrete (old)	27.89	0.2	2262	-	-
8	Pillar floor +1 concrete (new)	33.66	0.2	2363	-	-
9	Pillar floor +1 concrete (old)	32.71	0.2	2362	-	-
10	SAP 20+4 beam (new)	21.00	0.2	0	-	-
11	SAP 20+4 beam (old)	21.00	0.2	0	-	-
12	SAP 20+4 top slab concrete (new)	21.00	0.2	6875	-	-
13	SAP 20+4 top slab concrete (old)	21.00	0.2	6875	-	-
14	Infill (old)	4.99	0.3	1100	+150	-
15	SAP 16+4 equivalent material (for shells)	21.00	0.2	764	-	-
16	Front part concrete (new)	30.00	0.2	2500	-	-
17	Infill (new)	0.23	0.3	1100	-89	-
18	SAP20+4 equivalent material (for shells)	21.00	0.2	1546	-	-
19	Pillar floor 0 and -1 concrete (new)	27.63	0.2	2395	-	-
20	Pillar floor 0 concrete (old)	44.10	0.2	2362	+35	-
21	Pillar floor -1 concrete (old)	32.71	0.2	2362	-	-
22	Slab concrete old	21.00	0.2	2500	-	-
23	Slab concrete new	21.00	0.2	2500	-	-
24	Pillar head concrete	33.20	0.2	2363	-	-

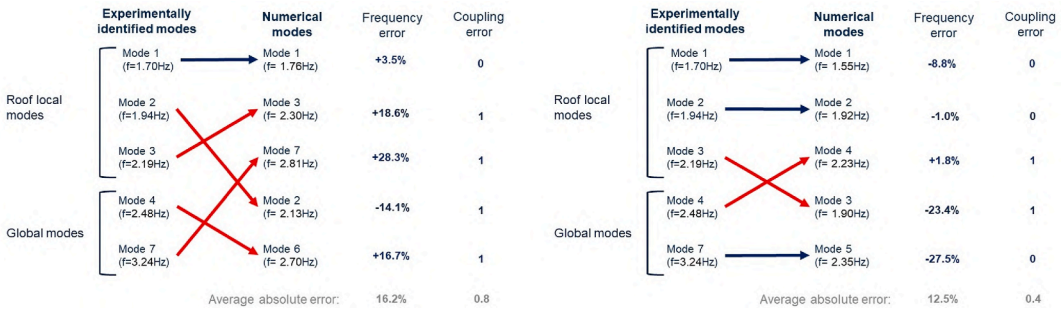


Fig. 14. Results of the model validation procedure for the initial configuration (a) and the final outcome (b).

This work presented an effective procedure to mitigate the mode inversion problem by leveraging sensitivity analysis to identify the most influential mechanical parameters and vibration modes for calibration. In particular, each parameter subset is updated using a dedicated cost function that considers only the modal discrepancies it governs, ensuring decoupled optimization. This targeted calibration prevents cross-parameter contamination, and help to reduce initial discrepancy which affect the reversal of vibration modes. Thus, through a recursive calibration process, the updated model has been validated and verified against Operational Modal Analysis results, ensuring.

- correct mode ordering (reduction of coupling error of 40 %) and;
- significantly reducing errors in modal parameters (reduction of natural frequency errors of about a 4 % over five modes and about 13 % over the three modes involved in the final updating of the calibration inputs).

Regarding the reference structure, three sources of uncertainty were identified, namely.

- the density of the roof;
- the stiffness of the infill walls and;
- the stiffness of the pillar heads.

The first two had a non-negligible influence on the dynamic response of the hall. In addition, another detected source of uncertainty was represented by the presence of an additional building that interacts with the Hall B and that is likely to influence the lateral stiffness of the structure, deriving in an impact on the vibration modes that expands laterally. This means affecting the 1st identified vibration mode (in terms of natural frequency), the 4th identified vibration mode (in terms of natural frequency and mode coupling, i.e., the mode is inverted), and the 7th identified vibration mode (in terms of natural frequency). Thus, as a future perspective, the modelling of the adjacent structure should be conducted and included in the analysis of Hall B, in addition, due to the residual discrepancies with experimental observations, definitive safety evaluation requires more advanced analysis. Once these discrepancies will be reduced, the high-fidelity model will be able to support nonlinear dynamic simulations to quantify structural capacity and identify damage-prone zones. In the meantime, the calibrated linear model enables preliminary assessment of stress intensification patterns, allowing identification of critical areas where additional investigation or reinforcement may be necessary.

CRediT authorship contribution statement

Erica Lenticchia: Writing – review & editing, Writing – original draft, Visualization, Validation, Software, Methodology, Investigation, Formal analysis, Data curation, Conceptualization, Supervision, Resources. **Gaetano Miraglia:** Writing – review & editing, Writing – original draft, Visualization, Validation, Software, Methodology, Formal analysis, Data curation, Conceptualization. **Jorge Alexis Cusicanqui Lopez:** Writing – review & editing, Visualization, Validation, Software, Formal analysis, Data curation. **Rosario Ceravolo:** Supervision, Resources, Project administration, Funding acquisition.

Declaration of competing interest

The authors declare the following financial interests/personal relationships which may be considered as potential competing interests: Rosario Ceravolo reports financial support was provided by The Getty Foundation of Los Angeles. Rosario Ceravolo reports financial support was provided by Società Committenza Piemonte (SCR). If there are other authors, they declare that they have no known competing financial interests or personal relationships that could have appeared to influence the work reported in this paper.

Acknowledgments

The present work was supported by the Keeping it Modern grant awarded by The Getty Foundation of Los Angeles (USA). The authors would also like to acknowledge the City of Turin, owner of the buildings and active partner of the project, and Società Committenza Piemonte (SCR), the Pier Luigi Nervi Foundation, in particular Arch. Cristiana Chiorino and Elisabetta Margiotta Nervi, and the laboratory technical staff of the MASTRLAB of Politecnico di Torino (DISEG) for the support in the experimental campaign, particularly Dr. Antonino Quattrone.

Data availability

Data will be made available on request.

References

[1] Filippo Lorenzoni, Filippo Casarin, Mauro Caldon, Kleidi Islami, Claudio Modena, Uncertainty quantification in structural health monitoring: applications on cultural heritage buildings, Mech. Syst. Signal Process. (2016), https://doi.org/10.1016/j.ymssp.2015.04.032, 66–67 (January):268–81.
[2] Charles R. Farrar, Keith Worden, An introduction to structural health monitoring, Philos. Trans. R. Soc. A Math. Phys. Eng. Sci. 365 (1851) (2007), https://doi.org/10.1098/rsta.2006.1928.
[3] Enrique García-Macías, Filippo Ubertini, Real-time bayesian damage identification enabled by sparse PCE-kriging meta-modelling for continuous SHM of large-scale civil engineering structures, J. Build. Eng. 59 (November) (2022) 105004, https://doi.org/10.1016/j.jobe.2022.105004.
[4] D' Altri, Antonio Maria, Vasilis Sarhosis, Gabriele Milani, Jan Rots, Serena Cattari, Sergio Lagomarsino, Elio Sacco, Antonio Tralli, Giovanni Castellazzi, Stefano de Miranda, Modeling strategies for the computational analysis of unreinforced masonry structures: review and classification, Arch. Comput. Methods Eng. 27 (4) (2020), https://doi.org/10.1007/s11831-019-09351-x.
[5] A.M. D'Altri, S. de Miranda, G. Castellazzi, B. Glisic, Numerical modelling-based damage diagnostics in cultural heritage structures, J. Cult. Herit. 61 (2023), https://doi.org/10.1016/j.culher.2023.02.004.
[6] P. Roca, The iscarsah guidelines on the analysis, conservation and structural restoration of architectural heritage, in: 12th International Conference on Structural Analysis of Historical Constructions, CIMNE, 2021, https://doi.org/10.23967/sahc.2021.290.

[7] Albert Cabané, Luca Pelà, Pere Roca, Laboratory and in-situ mechanical characterisation of masonry components by comparing destructive and minor destructive testing techniques, Constr. Build. Mater. 411 (2024), https://doi.org/10.1016/j.conbuildmat.2023.134474.

[8] Jacopo Ciambella, Gianluca Ranzi, Francesco Romeo, The pier Luigi Nervi's concrete structure of palazzetto dello sport: modeling and dynamic characterization, Struct. Concr. (2024). https://doi.org/10.1002/suco.202400320.

[9] Eduardo Diz-Mellado, Emilio J. Mascort-Albea, Rocio Romero-Hernández, Carmen Galán-Marin, Carlos Rivera-Gómez, Jonathan Ruiz-Jaramillo, Antonio Jaramillo-Morilla, Non-destructive testing and finite element method integrated procedure for heritage diagnosis: the seville cathedral case study, J. Build. Eng. 37 (2021) 102134.

[10] Davide Raviolo, Marco Civera, Luca Zanotti Fragonara, A comparative analysis of optimization algorithms for finite element model updating on numerical and experimental benchmarks, Buildings 13 (12) (2023) 3010, https://doi.org/10.3390/buildings13123010.

[11] John E. Mottershead, Michael Link, Michael I. Friswell, The sensitivity method in finite element model updating: a tutorial, Mech. Syst. Signal Process. 25 (7) (2011) 2275–2296, https://doi.org/10.1016/j.ymssp.2010.10.012.

[12] J.E. Mottershead, M.I. Friswell, Model updating in structural dynamics: a survey, J. Sound Vib. 167 (2) (1993) 347–375, https://doi.org/10.1006/jsvi.1993.1340.

[13] Davide Raviolo, Marco Civera, Luca Zanotti Fragonara, A bayesian sampling optimisation strategy for finite element model updating, Journal of Civil Structural Health Monitoring, February (2024), https://doi.org/10.1007/s13349-023-00759-5.

[14] Kyung K. Choi, Nam Ho Kim, Structural Sensitivity Analysis and Optimization 1, Springer New York, New York, NY, 2005, https://doi.org/10.1007/b138709.

[15] D. Novrikt, B. Teplyt, N. Shiraishi, Sensitivity analysis of structures: a review, in: The Fifth International Conference on Civil and Structural Engineering Computing Edinburgh, 1993, pp. 201–207, https://doi.org/10.4203/ccp.19.8.1. *Scotland, 17th - 19th August.*

[16] J.E. Mottershead, C. Mares, M.I. Friswell, S. James, Selection and updating of parameters for an aluminium space-frame model, Mech. Syst. Signal Process. 14 (6) (2000) 923–944, https://doi.org/10.1006/mssp.2000.1303.

[17] M. Imregun, W.J. Visser, D.J. Ewins, Finite element model updating using frequency response function data, Mech. Syst. Signal Process. 9 (2) (1995) 187–202, https://doi.org/10.1006/mssp.1995.0015.

[18] Q.W. Zhang, C.C. Chang, T.Y.P. Chang, Finite element model updating for structures with parametric constraints, Earthq. Eng. Struct. Dynam. 29 (7) (2000) 927–944, https://doi.org/10.1002/1096-9845(200007)29:7<927::AID-EQE955>3.0.CO;2-4.

[19] Zdeněk Kala, Libor Puklický, Variance-based methods for sensitivity analysis in civil engineering, in: Computational Structural Engineering, Springer Netherlands, Dordrecht, 2009, pp. 991–997, https://doi.org/10.1007/978-90-481-2822-8_111.

[20] B. Asgari, S.A. Osman, A. Adnan, Sensitivity analysis of the influence of structural parameters on dynamic behaviour of highly redundant cable-stayed bridges, Adv. Civ. Eng. 2013 (2013) 1–11, https://doi.org/10.1155/2013/426932.

[21] Quanjun Hua, Qing Chun, Chengwen Zhang, Nonlinear seismic analysis of city gate architectural heritages using a sensitive-based model updating method, J. Build. Eng. 89 (July) (2024) 109320, https://doi.org/10.1016/j.jobe.2024.109320.

[22] Pier Francesco Giordano, Filippo Ubertini, Nicola Cavalagli, Alban Kita, Maria Giovanna Masciotta, Four years of structural health monitoring of the san pietro bell tower in perugia, Italy: two years before the earthquake versus two years after, International Journal of Masonry Research and Innovation 5 (4) (2020) 445–467.

[23] Michael Friswell, John E. Mottershead, Finite Element Model Updating in Structural Dynamics, vol. 38, Springer Science \& Business Media, 1995.

[24] H. Sohn, C.R. Farrar, F.M. Hemez, J.J. Czarnecki, A Review of Structural Health Monitoring Literature : 1996-2001, Los Alamos National Laboratory Report, 2004. LA-13976-MS." *Los Alamos* LA-13976-M (LA-13976-MS).

[25] J.M.W. Brownjohn, Structural health monitoring of civil infrastructure, Philos. Trans. R. Soc. A Math. Phys. Eng. Sci. 365 (1851) (2007), https://doi.org/10.1098/rsta.2006.1925.

[26] Alessandro Cabboi, Carmelo Gentile, Antonella Saisi, From continuous vibration monitoring to FEM-based damage assessment application on a stone-masonry tower, Constr. Build. Mater. 156 (2017) 252–265.

[27] D.J. Ewins, Modal Testing: Theory, Practice and Application (Mechanical Engineering Research Studies: Engineering Dynamics Series), Research Studies Press Ltd, 2000.

[28] Bart Peeters, Guido De Roeck, Stochastic system identification for operational modal analysis: a review, J. Dyn. Sys., Meas., Control 123 (4) (2001) 659–667.

[29] Eleonora M. Tronci, Maurizio De Angelis, Raimondo Betti, Vittorio Altomare, Semi-automated operational modal analysis methodology to optimize modal parameter estimation, J. Optim. Theor. Appl. 187 (3) (2020), https://doi.org/10.1007/s10957-020-01694-x.

[30] John E. Mottershead, Michael Link, Michael I. Friswell, The sensitivity method in finite element model updating: a tutorial, Mech. Syst. Signal Process. 25 (7) (2011), https://doi.org/10.1016/j.ymssp.2010.10.012.

[31] R. Ceravolo, G. de Lucia, E. Lenticchia, G. Miraglia, A. Quattrone, F. Tondolo, E. Matta, et al., Challenges in the reuse and upgrade of pier Luigi Nervi 's structures, in: 12th International Conference on Structural Analysis of Historical Constructions SAHC 2020 Nel 29 Sep - 1 Oct, 2021, 2021, pp. 71–81.

[32] Erica Lenticchia, Amedeo Manuello Bertetto, Rosario Ceravolo, AE propagation velocity calculation for stiffness estimation in pier Luigi Nervi's concrete structures, Curved Layer. Struct. 8 (1) (2021), https://doi.org/10.1515/cls-2021-0010.

[33] Rosario Ceravolo, Paolo Faccio, Greta Bruschi, Cristiana Chiorino, Erica Lenticchia, Irene Matteini, Francesca Pasqual, Antonia Spanò, The Halls of Torino Esposizioni: from Conservation Management Planning to Future Use, 2024, pp. 77–89, https://doi.org/10.1007/978-3-031-67818-9_6.

[34] Claudio Greco, Pier Luigi Nervi. Dai Primi Brevetti Al Palazzo Delle Esposizioni Di Torino 1917-1948, Lucerne Quart Edizioni, Lucerna, 2008.

[35] R. Gargiani, A. Bologna, The rhetoric of pier Luigi Nervi: concrete and ferrocement forms. Treatise on Concrete, CRC Press LLC, 2016. https://books.google.it/books?id=vOjADAEACAAJ.

[36] G. Sammartano, G. Patrucco, S. Perri, R. Ceravolo, E. Lenticchia, A. Spanò, Documenting complexity for the 20TH century heritage: the enriched 3D models of the turin exposition NERVI'S halls digitization, ISPRS Annals of the Photogrammetry, Remote Sensing and Spatial Information Sciences (2021) 141–148, https://doi.org/10.5194/isprs-annals-VIII-M-1-2021-141-2021. VIII-M-1–2021 (August).

[37] G. Patrucco, S. Perri, G. Sammartano, E. Fillia, I. Matteini, E. Lenticchia, R. Ceravolo, A. Spanò, 3D models and NON-destructive investigations: towards a meeting in digital twins, Int. Arch. Photogram. Rem. Sens. Spatial Inf. Sci. XLIII-B2–2022 (May) (2022) 845–852, https://doi.org/10.5194/isprs-archives-XLIII-B2-2022-845-2022.

[38] Consiglio dei Ministri, Norme per l'esecuzione delle opere in conglomerato cementizio semplice o armato' (regulations for the execution of works in simple or reinforced concrete), in: Regio Decreto 16 Novembre 1939-XVIII, vol 2229, 1940. Suppl. Ord. alla Gazzetta Ufficiale, n. 92 del 18 aprile.

[39] International Committee CEN/TC 104/SC1, EN 12504-1:2019 Testing Concrete in Structures. Cored Specimens. Taking, Examining and Testing in Compression, 2019.

[40] International Committee CEN/TC 104/SC1, EN 12390-13:2021 Testing Hardened Concrete. Determination of Secant Modulus of Elasticity in Compression, 2021.

[41] BSI, EN1992-1-1:2023 Eurocode 2: Design of Concrete Structures. General Rules – Rules for Buildings, Bridges and Civil Engineering Structures, 2023.

[42] Erica Lenticchia, Rosario Ceravolo, Paola Antonaci, Sensor placement strategies for the seismic monitoring of complex vaulted structures of the modern architectural heritage, Shock Vib. (2018), https://doi.org/10.1155/2018/3739690, 2018.

[43] Erica Lenticchia, Gaetano Miraglia, Rosario Ceravolo, Dynamic identification of large thin shell structures in concrete, in: International Conference on Structural Analysis of Historical Constructions, 2023, pp. 777–787.

[44] P. Nervi, Tavole Salone B, Torino Esposizioni, Parma, 1947.

[45] Ministero delle Infrastrutture e dei Trasporti, Aggiornamento Delle «Norme Tecniche Per Le Costruzioni» NTC 2018, vol. 20, 2018 Roma.

[46] Saroj Phaiju, Prachand Man Pradhan, Experimental work for mechanical properties of brick and masonry panel, Journal of Science and Engineering 5 (2018), https://doi.org/10.3126/jsce.v5i0.22372.

[47] Francesca da Porto, Marco Donà, Nicolò Verlato, Giovanni Guidi, Experimental testing and numerical modeling of robust unreinforced and reinforced clay masonry infill walls, with and without openings, Frontiers in Built Environment 6 (2020), https://doi.org/10.3389/fbuil.2020.591985.

[48] André Furtado, Hugo Rodrigues, António Arêde, Humberto Varum, Mechanical properties characterization of different types of masonry infill walls, Front. Struct. Civ. Eng. 14 (2) (2020), https://doi.org/10.1007/s11709-019-0602-y.
[49] L. Cavaleri, M. Papia, G. Macaluso, F. Di Trapani, P. Colajanni, Definition of diagonal Poisson's ratio and elastic modulus for infill masonry walls, Materials and Structures/Materiaux et Constructions 47 (1–2) (2014), https://doi.org/10.1617/s11527-013-0058-9.
[50] S. Albanesi, T. Albanesi, F. Carboni, The influence of infill walls in r.c. Frame seismic response, in: High Performance Structures and Materials, vol. 7, 2004.
[51] ANSYS, Inc, Ansys APDL, 2024.
[52] MathWorks, MATLAB Version: (2023b), The MathWorks Inc., Natick, Massachusetts, 2023.